國 立 交 通 大 學

物理研究所

碩 士 論 文

刮刀塗佈技術於有機太陽能電池與多層結構有機鄰近感測器的應用

Blade coating for polymer solar cells and multilayer polymer photo-detectors

系 所 別：物理研究所碩士班

研 究 生：張玉函 (Yu-Han Chang)

指導教授：孟心飛 教授 (Prof. Hsin-Fei Meng)

洪勝富 教授 (Prof. Sheng-Fu Horng)

中華民國九十八年六月

刮刀塗佈技術於有機太陽能電池與多層結構有機鄰近感測器的應用

Blade coating for polymer solar cells and multilayer polymer photo-detectors

研究生：張玉函　　Student：Yu-Han Chang

指導教授：孟心飛 教授　　Advisor：Prof. Hsin-Fei Meng

國 立 交 通 大 學

物理研究所

碩 士 論 文

A Thesis

A Dissertation Submitted to Institute of Physics College of Science

National Chiao Tung University

in partial Fulfillment of the Requirements

for the Degree of

Master

in

Physics

June 2009

Hsinchu, Taiwan, Republic of China

中華民國九十八年六月

刮刀塗佈技術於有機太陽能電池與多層結構有機鄰近感測器的應用

國立交通大學物理研究所碩士班

學生：張玉函　　指導教授：孟心飛 教授

洪勝富 教授

摘要

本研究採用施子(donor)材料- poly(3-hexylthiophene) (P3HT)以及受子(acceptor)材料-(6,6)-phenyl-C61-butyric acid methyl ester (PCBM)，將其均勻混合於甲苯(toluene)溶液，利用刮刀塗佈技術製作塊材異質接面有機太陽能電池與光感測器。利用刮刀塗佈製程使能夠有序排列形成施子-受子的自組裝結構以提升載子的傳輸效率。

本研究之有機太陽能電池達到高能量轉換效率(power conversion efficiency, PCE) 3.8%，相較於一般於甲苯溶液以旋轉塗佈(spin coating)製程效率 2.6%，整體元件效益提升達 46%。於光感測元件的研究，透過刮刀製程應用於多層結構設計，將元件暗電流密度降低至 10^{-5} mA/cm^2，比單層旋轉塗佈製程元件可降低其暗電流值的 100 倍，有效提升整體元件感測靈敏度。

關鍵字：共軛高分子、塊材異質接面、太陽能電池、光偵測器、P3HT、PCBM

Blade coating for polymer solar cells and multilayer polymer photo-detectors

Institute of Physic
National Chiao Tung University

Student: Yu-Han Chang Advisors: Prof. Hsin-Fei Meng

Prof. Sheng-Fu Horng

Abstract

A donor-acceptor blend for bulk hetero-junction polymer solar cells and polymer photo-detectors are studied by using poly(3-hexylthiophene) (P3HT) as the donor and (6,6)-phenyl-C61-butyric acid methyl ester (PCBM) as the acceptor. Desired ordered donor-acceptor self-organization is achieved by blade coating with high carrier mobility.

The polymer solar cell with power conversion efficiency (PCE) is 3.8% in this study, which is 46% higher than that obtained by spin coating in toluene solution (2.6%). In addition, the multilayer photo-detector can be achieved by blade coating to reduce dark current density to 10^{-5} mA/cm^2. That is about 100 times lower than that of single layer structure by spin coating, enhancing the sensitivity.

Key word: conjugate polymer, bulk hetero-junction, polymer solar cell, polymer photo-detector, P3HT, PCBM

致　謝

悄悄的我走了，正如我悄悄的來；
我揮一揮衣袖，不帶走一片雲彩。

猶記得第一次細讀這首耳熟能詳的「再別康橋」，腦海中盪漾著〝不帶走一片雲彩〞如此的告別多麼灑脫自得！作者寄情於康橋景致的離情依依，給了我無限的感動！回顧研究生涯兩年來的時光，腦海中的回憶如相片膠捲般一幕幕浮現，實驗室這個大家庭幾乎是這些年來研究生活的全部，精采的故事很多，一起難過、一起歡笑的畫面至今仍記憶猶新。離別的時刻，由衷地感謝每一位陪伴我一路走來的師長與好友，此刻帶走的是各位給我的一片情誼！

首先感謝的是實驗室兩位大家長 孟心飛教授和 洪勝富教授，感謝兩位老師在研究道路上指引我重要的方向。特別是我的指導教授-孟老師，還記得放榜之際第一次邀請您擔任指導教授的場景，如今轉眼我已完成了學業。兩年多來的日子感激老師悉心的指導並給予我許多的學習機會，養成應有的研究精神與態度，豐富的學習經驗充實了我的碩士研究生涯。

「有機半導體實驗室」就像個熱鬧的大家庭，在嚴謹的研究要求之下，也不乏許多開心愉快的氣氛。尤其幾位實驗室重要的博士班學長姊們一直是我學習的好榜樣，宇強學長、家銘學長、建成學長在研究上總不吝分享豐富的研究經驗，平常也很照顧學弟妹；明錕學長和仁君學姊在專業研究領域上總熱心給予學弟妹們盡可能的協助；以及俊宇學長、銘志學長、韻茹學姊平日開心愉快的笑容爲實驗室營造不少輕鬆愉快的氣氛。

LED組更是這大家庭裡一群令人難忘的家人。兩年來信榮學長就像是LED組一把穩固的大傘呵護我們在研究之路上一步一步地成長，實驗上實事求是的要求以及親切耐心的討論分享，從摸索學習到放手讓我們每一個人擁有各自研究領域的一片天。猶

記每回小組會議之後一群小毛頭圍著你討論實驗方向的場景，是腦海裡深刻的畫面；這些年來無限的感激化為一句深深的謝謝你！冠成學長總是細心地給予學弟妹許多的關心，一路陪伴我們走來，是學長更是知心的好友。恩禎學長就像個鄰家大哥一般，無論研究上或生活上的事物總樂於與人分享，有你的地方就有歡笑，是我們組內最寶貝的開心果。還有六年的同窗好友重麟、青春洋溢的紘瑋、活潑搞笑的佳達、貼心好男人形象的文興、溫柔婉約的季庭、外向健談的勝佳、中肯踏實的嘉佑、對凡事都很認真的宗祐以及認真上進的碩一學弟韋嵐，多麼難得的緣份讓我們齊聚人生中寶貴的兩年，因為有你們讓我的研究生活多采多姿，滿滿的回憶裡永遠記得大家燦爛的笑容與開懷的笑聲。

最後我要感謝我摯愛的家人，視我己出的姑媽 張艾倫女士和伯父 張化民先生，謝謝你們在我成長過程中無微不至的照顧與關愛。媽媽 陳金貴女士在我求學階段默默地支持與鼓勵我。很感恩我生長在一個未必健全卻充滿幸福的家庭，因為擁有家人許多的溫暖讓我即使面對困境也能勇敢的向前走，我愛你們！我是一個幸福的女孩，在人生的旅程上有著貼心的男友兆仟、知心的好姊妹詩敏，與你們一起，我可以自在地開心的大笑、難過的大哭，感謝你們始終陪伴著我！

要感激的人真的很多，謝謝老天爺給我雖不富有卻幸福的家庭、雖不完美卻值得珍惜的人生！畢業是人生一個階段的結束，我將帶著更多的祝福與期望邁向下一個人生嶄新的新頁。

交通大學物理研究所

張玉函 2009年七月

Contents

Part 1 Efficient polymer solar cells by blade coating

Part 2 Multilayer polymer photo-detectors

Tables

Part 1 Efficient polymer solar cells by blade coating

Part 2 Multilayer polymer photo-detectors

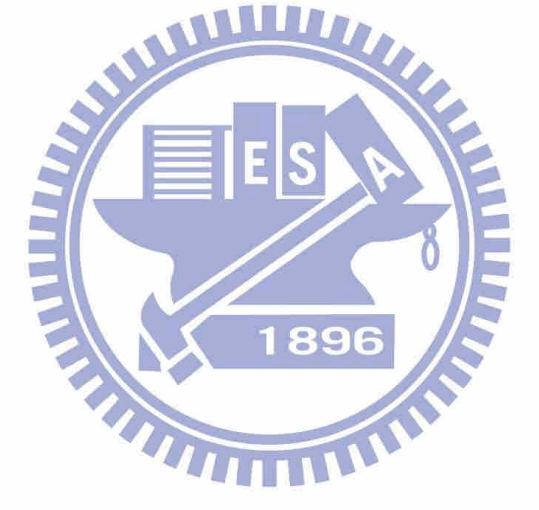

Figures

Part 1 Efficient polymer solar cells by blade coating

Part 2 Multilayer polymer photo-detectors

Part 1 Efficient polymer solar cells by blade coating

Chapter 1 Introduction

1.1 Background of research

1.1.1 Energy resources and solar energy

People use the major source of energy such as the petroleum, natural gas, and coal in the world. According to the analysis report of energy resource of the world from British Petroleum, that shows the surplus usable amount of petroleum about 40 years, the natural gas about 60 years, and the amount of coal about 200 years after 2000 year. That indicates the less resource remaining in the soon after.

The people depend on the petrifaction energy that shown from who use the energy over 85% for global resource. At the same time, the transformation of global weather is an important subject in the international society. A main problem of weather is the greenhouse effect, which results largely climatic changes from dischargeable carbon dioxide (CO_2) that comes from the burn petrifaction energy. Therefore, how to reduce the amount of carbon dioxide and to improve the greenhouse effect is a common goal in the whole world.

For decreasing the discharge of carbon dioxide, seeking out the replacement is an essential solution unless economizing on energy usage. As revealed by Fig. 1-1-a, the energy requirement is more and more in the future. So the energy resource is replaced by solar energy that is a future tendency.

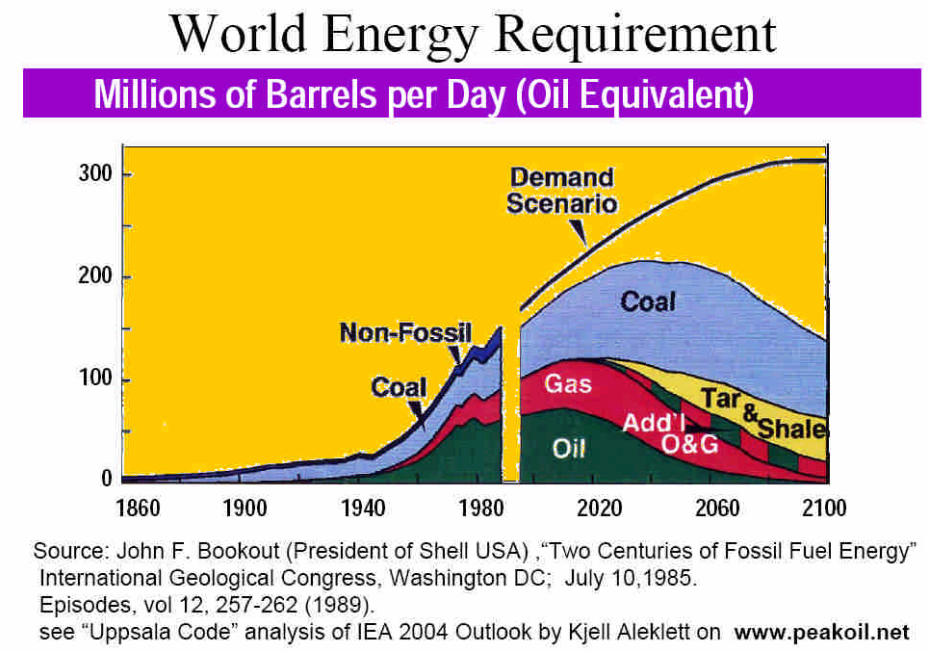

Fig. 1-1-a The requirement of energy and the tendency of several energy decreasing

There are a lot of unique properties of solar energy such as 'universality' means that it exists in everywhere; 'clean energy' means it does not produce pollution; 'no time-limit usage' means that the sun has existed for 4.5 billion years, and it will exist about ten billion years. Furthermore, the solar energy is a powerful energy, which provides for usage amount is almost thirty thousand times larger than amount of consumption in the world [1]. As can be seen, how to use the solar energy is the most important topic at present.

1.1.2 Development of solar cells

Recently the solar cell has become an important research subject. The solar cells could be classified as several types of silicon solar cells, inorganic compound solar cells, and organic solar cells according to the materials.

The first inorganic solar cell with power conversion efficiency (PCE) is 6% that was fabricated using silicon by Bell Laboratory in 1945 year [2]. After so many years, the PCE of single crystal silicon solar cell has achieved 24.7% in the academia today [3]. At present,

the silicon solar cells could be separated three types that are single crystal solar cells, polysilicon solar cells, and amorphous silicon solar cells. The single crystal and polysilicon solar cells have the similar fabrication, and the amorphous silicon solar cell is different from them. The amorphous silicon solar cell is a thin film solar cell with the advantages of large area and the low cost that was brought up by D. E. Carlson et al. in 1976 year [4]. The academia could achieve the PCE to 14.5% nowadays [5]. And the thin film solar cell was fabricated by compound material such as CdTe, $CuInSe_2$ (CIS), and $Cu(In,Ga)(S,Se)_2$ with the PCE 19.2% recently [6].

The single crystal solar cell and the polysilicon solar cell are popular in the market. The single crystal solar cell is almost used in power-station, lighting, and so on. And the polysilicon solar cell is used in low power application because of it is easy to fabricate and the low cost. Besides, the amorphous silicon solar cell has the many electronic products generally since it is the lowest cost in fabrication.

The solar cell properties have stably grown up in the past years. The cost of fabrication is low day by day through development continuously. However, the usage of solar energy is under 0.1% of all the resource consumption so far. It is to know that the high cost of the inorganic solar cell even the technology is mature. Therefore, to develop the fresh type of solar cell is a key point in the future.

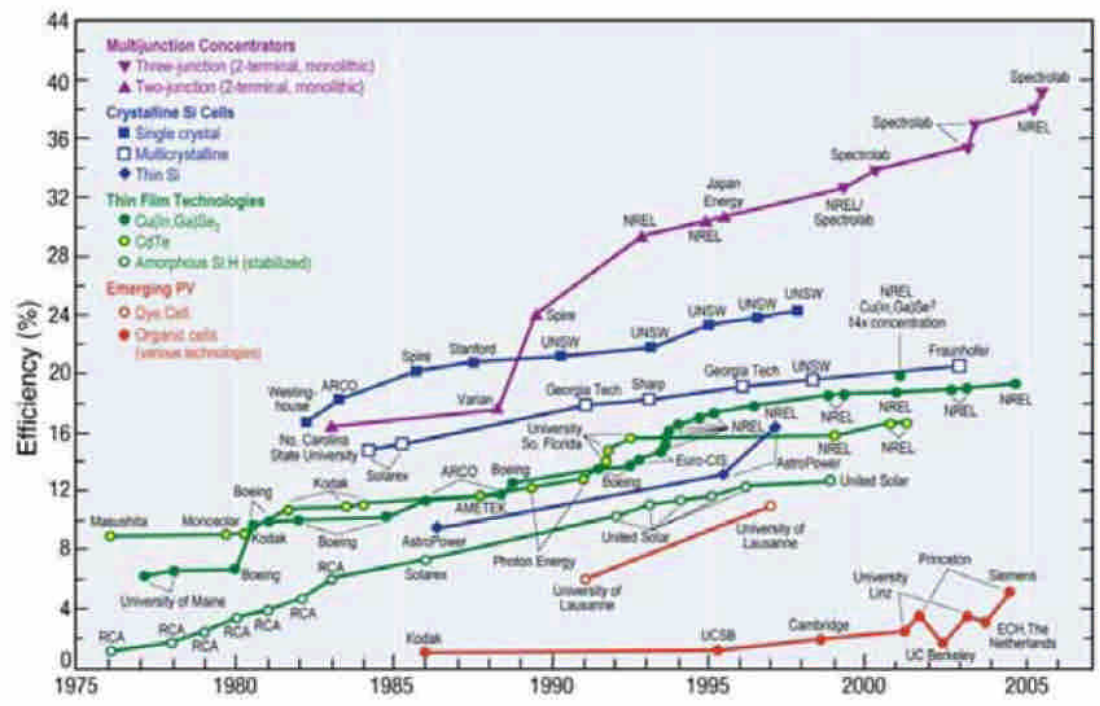

Fig. 1-1-b The development of power conversion rate for several solar cell types [7]

1.1.3 Development of polymer solar cells

The organic solar cell was paid attention to heavily research in recent ten years, the device structure advances from single layer to bilayer hetero-junction structure, bulk hetero-junction, and ordered bulk hetero-junction, shown in Fig. 1-1-c. The development tends to increase the transmission path and transmission rate of carriers.

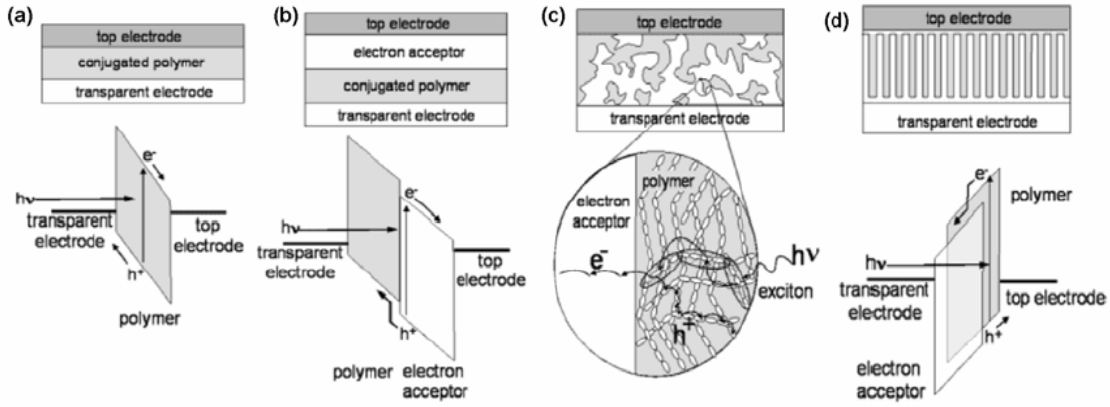

Fig. 1-1-c The structures development of organic solar cells [8]

The structure of bilayer hetero-junction is used the energy band gap offset of two component materials to induce the exciton separation, that effectively solves the problem of electron and hole could not separate by thermal energy for single layer structure in the room temperature. Finally separated carriers are collected by electrodes respectively. But the power conversion rate is not high enough because of the carrier separation region is too less (just only in the interface) to achieve high efficiency. The bulk hetero-junction structure increases the efficiency due to the improvement of separation region. After separation, some of the carriers would drift to the dead end and are unable collected by electrodes. For this reason, the next development structure is ordered bulk hetero-junction, that successful solves the problem.

The suitable idea is that integrated hetero-junction and bulk hetero-junction structures of bilayer to become an ordered bulk hetero-junction structure, as revealed by Fig. 1-1-c (d). That structure retains advantages not only the large separation area of bulk hetero-junction, but also the direct transmission path for carriers of bilayer hetero-junction structure. Hence, the ordered bulk hetero-junction is the most effective structure to increase the carrier transmission rate.

So far the organic solar cell could be discriminated from the types of material for small molecular solar cells, polymer solar cells, and dye-sensitized solar cells (DSC).

The small molecular solar cell with 1% was brought up by C. W. Tang in 1986 [9], that was fabricated with copper phthalocyanine (CuPc) and perylenetetra carboxylic-acid debenzimidazole (PV) materials by thermal evaporation. The device structure is to use the bilayer hetero-junction structure to increase the carrier separation rate.

The materials for polymer solar cell are the conjugate polymers because they could be dissolved in solvents and could be made by many cheap technologies like spin coating,

ink-jet printing, blade coating, and so on. The polymer solar cell was developed in 1994 year, which was made by blending polymers and C_{60} as the active layer [10]. There was a key idea of the bulk hetero-junction structure that enable expanded the separation region of carriers to everywhere in organic layer, as shown in Fig. 1-1-d. An important opinion about the structure of organic layer influences the development of polymer solar cells subsequently.

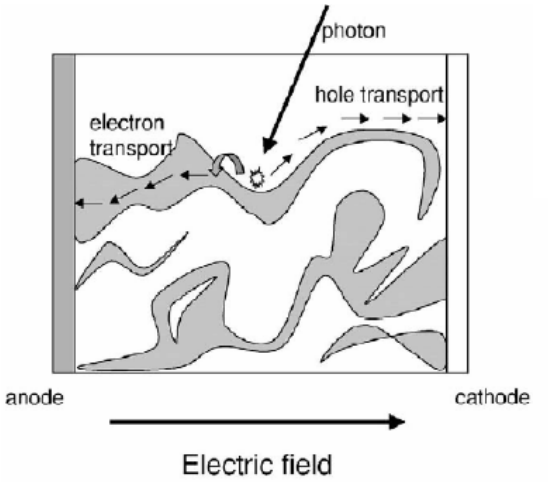

Fig. 1-1-d Bulk hetero-junction structure [11]

The first polymer/polymer hetero-junction solar cell with PCE 1% under monochromatic luminescence was presented by Yu et al [12] and Halls et al [13] in 1995 year. The materials were polymer compound of CN-PPV (acceptor) and MEH-PPV (donor). So far the polymer solar cell is used with blending system of P3HT and PCBM with the highest PCE to 6% [14].

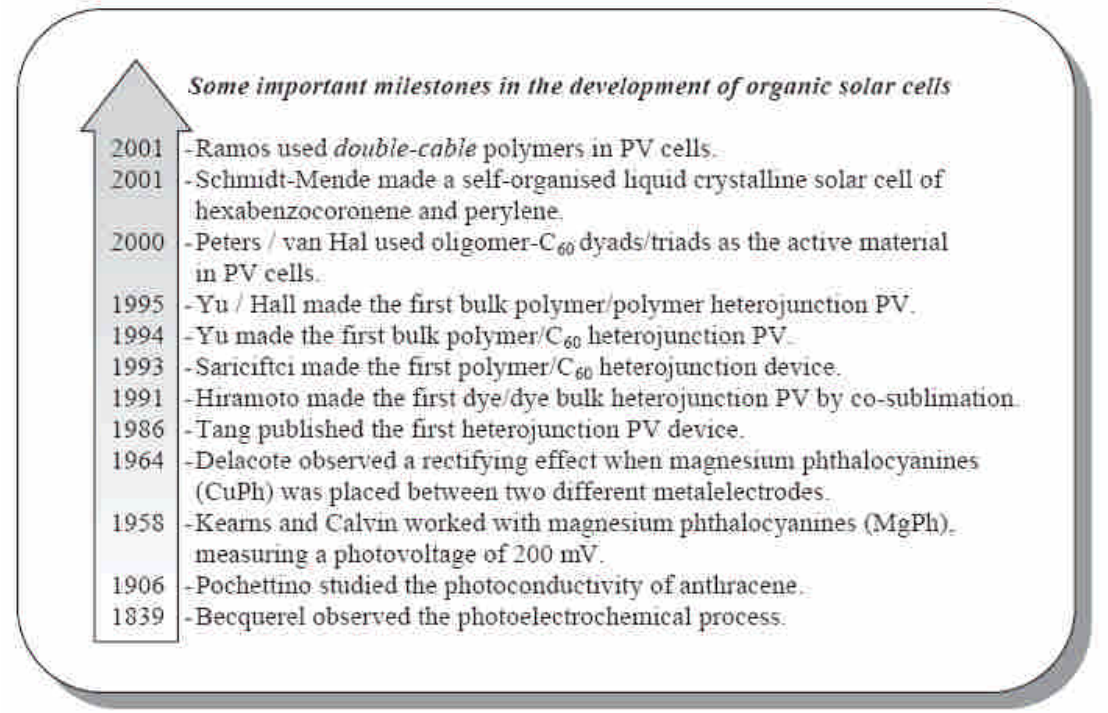

Fig. 1-1-e The table of development for polymer solar cells [15]

The DSC with PCE 7.1% was presented by M. Grätzel et al in 1991 year [20]. The DSC is the hybrid solar cell, that fabrication is coating the sensitizer on porous TiO_2 and using the electrolyte as medium of hole transmission, as Fig. 1-1-f. The other name of DSC is ‘Grätzel cell’ or ‘photo-electro-chemical cell’ (PEC cell). According to the report [21], the DSC with PCE achieved 12% from Konarka Flexible Plastic DSC Laboratory in 2005 year. The Konarka Company expects that will expand the products scope to enter the electronic market like PDA.

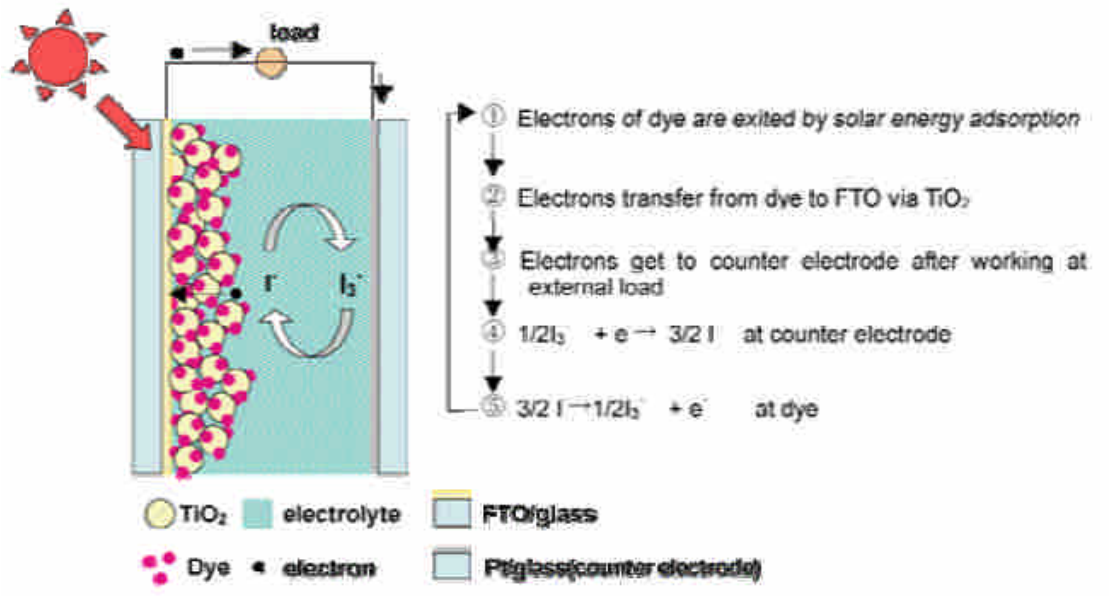

Fig. 1-1-f The working principle of DSC [19]

1.2 Motivation of research

1.2.1 Opportunity for polymer solar cells

There is a very low ratio of the solar energy usage that compares with the petrifaction energy. The main cause of the inorganic solar cell products is the highly expense in the market due to the fact that the usage is not popular today. Consequently, the organic solar cell is paid more and more attention recently because of the remarkably cheaper coating process than inorganic products even if the stability and the efficiency are not as better as inorganic solar cell.

In the many types of solar cell research, the development of DSC is mature than others since it is conformed the properties of the cheap price, the high efficiency, and the reliability has achieved to several thousand hours. But there is a difficult problem for the device packaging with the electrolyte inside although it is a lot of advantageous positions. The safety and convenience of DSC products are influenced by such serious problem. The

other two types of small molecular solar cell and polymer solar cell are tend to stable development since the advantages of the low cost and the easy processes of fabrication. However the fabrication of small molecular solar cell needs the expensive evaporator equipment and the complex process than polymer solar cell. Furthermore, the small molecular solar cell is not easy to scale up to large sizes.

In terms of the many reasons, recently conjugate polymer solar cells have attracted great interests due to their unique properties such as easy solution process for large-area, light weight, and mechanical flexibility. The polymer bulk hetero-junction cells have interpenetrating networks of electron donors and acceptors, resulting in an efficient exciton dissociation and high photo-currents with PCE about 5% [16] [22]. Although the efficiency is not as high as that of inorganic solar cells, the potential of low-cost and roll-to-roll process on flexible substrates makes the polymer solar cells attractive as the solution to the serious energy challenges.

1.2.2 Advantage of blade coating application in polymer solar cells

To date the most of efficient polymer solar cells are made by spin coating, which causes serious material waste and raises the cost dramatically. In addition, the spin coating process is not easy to scale up to very large sizes up to meters and is incompatible with the roll-to-roll process for high throughput production. Furthermore one major problem of the spin coated polymer solar cell is that a very toxic high boiling point organic solvent like dichlorobenzene (180.5 ℃) or chlorobenzene (131 ℃) is necessary for high efficiency. The high boiling point allows a slow drying process where the donor and acceptor molecules self-assemble into an interpenetrating network [16]. The high toxicity of dichlorobenzene and chlorobenzene makes the mass production environmentally unfriendly, and the slow drying process delays the production throughput.

Although there have been researches on fabrication processes, including ink-jet printing [23], screen printing [24], spray coating [25], and blade coating [28], the development of alternative solution coating methods compatible with the low-cost and environmentally friendly mass production remains a crucial problem [27]. Since there is no necessary for organic layers to be structured by printing in organic solar cells, blade coating for large area fabrication has been proved to be the better way [28]. The film thickness by blade coating can be reduced to nanometer scale by carefully controlling the fabrication parameters such as the solution concentration, the blade gap, and the blade coating speed.

We verified the feasibility of blade coating for high efficiency polymer light-emitting diodes [29]. Unlike spin coating, the area can be easily scaled up and the material usage is almost 100% in blade coating. In this work, blade coating is applied to poly(3-hexylthiophene) (P3HT) and (6,6)-phenyl-C61-butyric acid methyl ester (PCBM) blend in the toluene solution which has a lower boiling point (110 ℃) and is less toxic. High efficiency is achieved from toluene solution without the slow solvent evaporation process.

1.3 Thesis frameworks for part 1

Chapter 1 Introduction
Introduced the background, motivation, and purposes of research

Chapter 2 Theory
Introduced the fundamental principles

Chapter 3 Method
Introduced the experimental processes and materials

Chapter 4 Result
Discussed the experimental results

Chapter 5 Conclusion
Summary the important results

Y. H. Chang, S. R. Tseng, C. Y. Chen, H. F. Meng, E. C. Chen, S. F. Horng, C. S. Hsu,' Polymer solar cell by blade coating', Organic Electronics (2009) in press.

Chapter 2 Theory

2.1 Fundamental principles of solar cells

2.1.1 Equivalent circuit

For Fig. 2-1-a, the conventional solar cell is designed as the PN junction structure. There is a single energy band gap E_g between materials, and the PN junction connects with a load. When the solar cell absorbs the light with incident energy larger enough than the band gap, the excitons (electron-hole pairs, EHP) would be induced and diffuse to everywhere in the materials. Supposing that the excitons do not recombine before diffuse to the depletion region, and they would be separated by build-in electric field, as Fig. 2-1-b shown. A exciton transforms into a electron and hole carrier that are collected by the electrodes respectively and produces a reverse current in the diode. When the load is turned off, the measurement would get the current that is transformed from the absorption of light source, called the photocurrent.

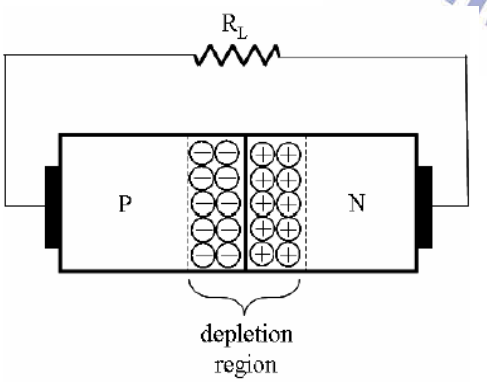

Fig. 2-1-a The conventional solar cell with the PN junction structure

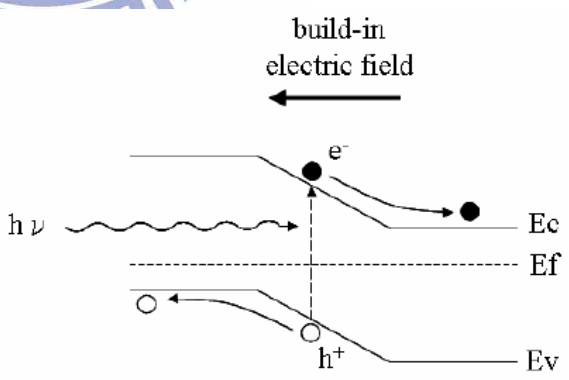

Fig. 2-1-b The excitons are separated by the build-in electric field

The ideal equation of diode as Eq. 2-1, indicates that the current-voltage characteristics (I-V characteristics). The ideal I-V is called dark current that shows the commutation property of current. It is induced a stable photocurrent under the steady illuminant.

According to the superposition principle for I-V characteristic and the stable photocurrent that obtains the I-V characteristics curve (as Fig. 2-1-c) and the I-V equation (as Eq. 2-2) under a stable power of light source. And the equivalent circuit of the ideal solar cell is shown in Fig. 2-1-d. A diode symbol represents the PN junction and I_{ph} represents the photocurrent that under the stable power of illumination. However, there are realistic effect of the high-level injection in the PN junction and the recombination of net carrier. For the reasons, it is must added the ideal factor 'n' to correct as Eq. 2-3.

$$I_d = I_0\left[\exp\left(\frac{qV_d}{k_BT}\right)-1\right] \quad \text{(Eq. 2-1)}$$

$$I = I_d - I_{ph} = I_o\left[\exp\left(\frac{qV_d}{k_BT}\right)-1\right] - I_{ph} \quad \text{(Eq. 2-2)}$$

$$I_d = I_0\left[\exp\left(\frac{qV_d}{nk_BT}\right)-1\right] \quad \text{(Eq. 2-3)}$$

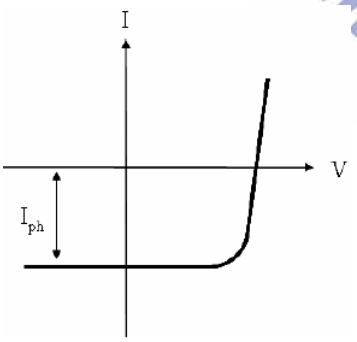

Fig. 2-1-c I-V characteristics of the ideal solar cell under illumination

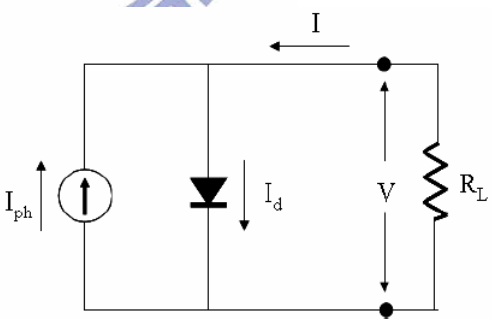

Fig. 2-1-d Equivalent circuit of the ideal solar cell

In fact, there are problems about series resistance R_s and the leakage current so the equivalent circuit must correct again. The R_s can be attributed to the semiconductor bulk and ohmic contact for the electrode in the solar cell device. Fig. 2-1-e shows an equivalent circuit of the realistic solar cell, R_s indicates the total series resistance from the generation

factor of materials or experiments, and the R_{sh} indicates the shunt resistance. The R_s and R_{sh} are shown as Eq. 2-4 and Eq. 2-5 under illumination [30].

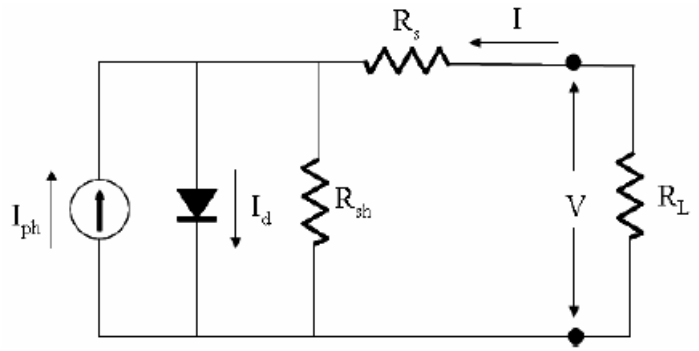

Fig. 2-1-e Equivalent circuit for a real solar cell

$$R_s = \lim_{V_{out}\to\infty}\left\{\frac{dV_{out}}{dI_{out}}\right\} \quad \text{(Eq. 2-4)}$$

$$R_{sh} \approx \frac{dV_{out}}{dI_{out}}\left(V_{out}=0\right), \quad R_s << R_{sh} \quad \text{(Eq. 2-5)}$$

$$I = I_0\left\{\exp\left[\frac{q\left(V-IR_s\right)}{nk_BT}\right]-1\right\}+\frac{V-IR_s}{R_{sh}}-I_{ph} \quad \text{(Eq. 2-6)}$$

Therefore, the I-V equation of the realistic solar cell shows in equation 2-6. Fig. 2-1-f shows the I-V characteristics of real solar cell, which is considered with the diode properties and the effect for R_s and R_{sh}. The curve indicates the current is not a stable value under the reverse bias, and the current would exchange with the voltage under the positive bias. At the same time, the I-V characteristic is not a vertically rising line. All of the appearance for I-V characteristics is produced from the R_s and R_{sh}. The I-V characteristics respond to the efficiency of the solar cell devices.

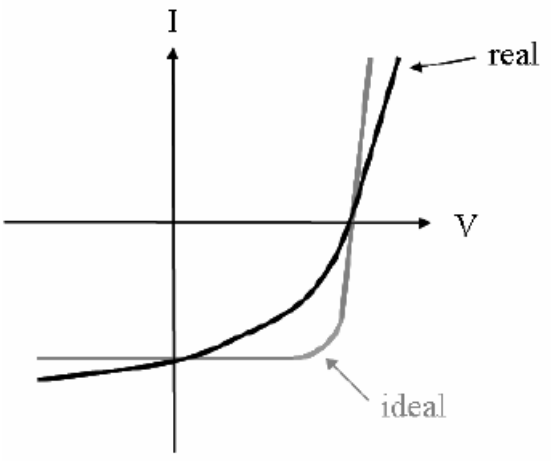

Fig. 2-1-f I-V characteristics of the ideal solar cells and the real solar cells under illumination

$$I = I_0\left\{\exp\left[\frac{q(V - IR_s)}{nk_BT}\right] - 1\right\} - I_{ph} \quad \text{(Eq. 2-7)}$$

$$I = I_0\left[\exp\left(\frac{qV}{nk_BT}\right) - 1\right] + \frac{V}{R_{sh}} - I_{ph} \quad \text{(Eq. 2-8)}$$

I-V characteristic equation (Eq. 2-6) of equivalent circuit for solar cells could be simplified to Eq. 2-7 and Eq. 2-8. The I-V characteristic is influenced by R_{sh} when the diode current I_d is much larger than the leakage current V_d/ R_{sh}, then R_{sh} became a slight factor simultaneously. Therefore the Eq. 2-6 could be replaced by Eq. 2-7.When the I_d is equal to the Vd/ R_{sh}, then R_{sh} is a notable factor under the weak illuminant, so the Eq. 2-6 could be correct to Eq. 2-8.

The Fig. 2-1-g shows the I-V characteristics of the silicon solar cell with a stable photocurrent density under a stable illuminant. In Fig. 2-1-g (a) the R_s not only influences the fill factor (FF, introduction in 2-1-2 section) but also exchanges a tendency toward short-circuit current (I_{sc}, introduction in 2-1-2 section) becomes smaller and R_s becomes larger. For the Fig. 2-1-g (b), the FF is influenced by the R_{sh} and the turn on voltage is

slightly decreased with the R_{sh} is dropped off.

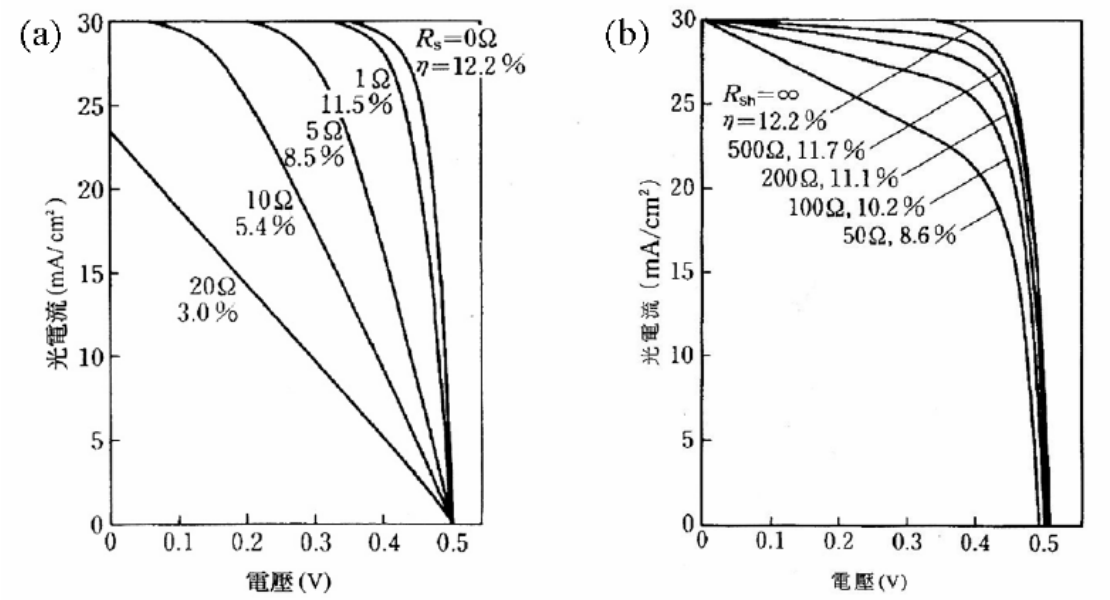

Fig. 2-1-g The I-V characteristics of a solar cell of (a) different R_s and (b) different R_{sh} [31]

2.1.2 Basic parameters

The fundamental parameters of solar cell are the short-circuit current (I_{sc}), the open-circuit voltage (V_{oc}), the fill factor (FF), the power conversion efficiency (PCE), and the external quantum efficiency (EQE). Fig. 2-2-a shows relation between the I-V characteristic and the parameter definition.

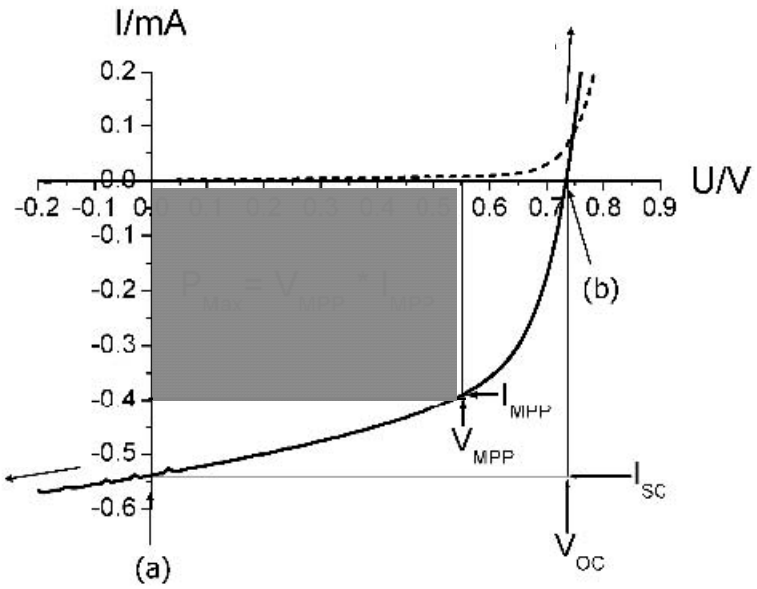

Fig. 2-2-a The relation between the I-V characteristics and the parameter definition of a solar cell [32]

A. Short-circuit current (I_{sc})

From the I-V characteristics, the solar cell could be measured with I-V relation by changing the load under a stable illumination. When the load is equal to zero, the current is called short-circuit current, I_{sc}, as shown in Fig. 2-2-a point (a). Without consideration of leakage current, the I_{sc} indicates the photocurrent as $I_{sc} = I_{ph}$.

B. Open-circuit voltage (V_{oc})

When the load tends to be unlimited and the current is equal to zero, the voltage is called the open-circuit voltage, V_{oc}, as the point (b) in Fig. 2-2-a. The working region of the solar cell is in the fourth quadrant, which is the load exchange from zero to large limit.

C. Fill factor (FF)

In the working region of a solar cell, there is a maximum output power (P_{max}) under a particular load. According to the P_{max}, that defines the maximum power point values of

current and voltage that are indicated as I_{mpp} and V_{mpp} separately shown in Fig. 2-2-a. The P_{max} is equal to multiply the two values as Eq. 2-9. FF is a ratio between P_{max} and $I_{sc} \times V_{oc}$ as Eq. 2-10. FF indicates the turn-on properties of the I-V characteristics in the fourth quadrant and can help us to know the R_s and R_{sh} how to influence on solar cell.

$$P_{\max} = I_{\max} V_{\max} \quad \text{(Eq. 2-9)}$$

$$FF = \frac{P_{\max}}{I_{sc} V_{oc}} = \frac{I_{\max} V_{\max}}{I_{sc} V_{oc}} \quad \text{(Eq. 2-10)}$$

D. Power conversion efficiency (PCE)

The power conversion efficiency is a ratio with the maximum output power and the power of incident illuminate. The P_{max} could be obtained from the I_{sc}, V_{oc}, and FF as shown in Eq. 2-11.

$$\eta = \frac{P_{max}}{P_{in}} = \frac{FF \times V_{oc} \times I_{sc}}{P_{in}} \quad \text{(Eq. 2-11)}$$

E. External quantum efficiency (EQE)

The external quantum efficiency (EQE) indicates conversion efficiency between the incident photon numbers and the induced photocurrents. It is a ratio with the output electron numbers and the incident photon numbers. As shown in Eq. 2-12, the external quantum efficiency is relative to the wavelength of incident light, the power, and the I_{sc}, and has no relationship with the V_{oc} and FF. The value of the I_{sc} is relative to the EQE. The EQE could be indicated with Eq. 2-13 in the bulk hetero-junction structure.

$$EQE = \frac{OutputElectron}{InputPhoton} = \frac{1240 \times I_{sc}}{P_{in} \times \lambda(nm)} \quad \text{(Eq. 2-12)}$$

$$\eta_{EQE} = \eta_A \times \eta_{ED} \times \eta_{CS} \times \eta_{CC} \quad \text{(Eq. 2-13)}$$

Fig. 2-2-b shows the EQE that could be separated by the four parameters with η_A, η_{ED}, η_{CS}, and η_{CC} through the process from the photon absorption to the carrier collection. The sequence of the four factors is expressed the conversion process from photons to electrons. The main factors to affect the EQE are η_{CS} and η_{CC}.

Symbol	Appellation	Effect
η_A	Absorption efficiency	The efficiency of absorbed illumination for devices.
η_{ED}	Exciton diffusion efficiency	The efficiency of the exciton diffusion to the material interface.
η_{CS}	Carrier separation efficiency	The efficiency of the exciton separation in the material interface.
η_{CC}	Carrier collection efficiency	The efficiency of the carrier transmission and collection by the electrodes.

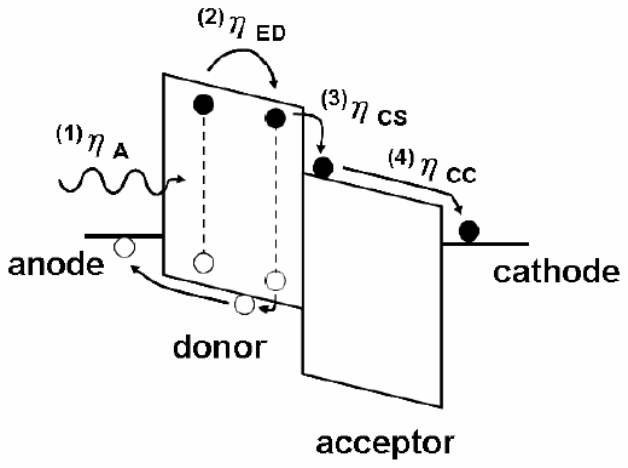

Fig. 2-2-b The energy band of the material interface and the electrode in short-circuit condition

2.2 Characteristics of conjugate polymer materials

2.2.1 Development

The polymer semiconductor was jointly discovered by the A. G. MacDiarmid, A. J. Heeger, and Hideki Shirakawa since 1977 year. They used the polyacetylene with doping the iodine. The degree of electric conduction was increased over one hundred million times [33]. After about thirty years, there are a lot of the important research results for conjugate polymer. The three of the scientists have obtained the chemical Nobel Prize in 2000 year. The conjugate polymers are many developments in the various photovoltaic regions, and will prosperous expand in the future.

2.2.2 Photovoltaic property

The monomer is a fundamentally chemical structure. It is usually composed by the elements like carbon, hydrogen, oxygen, and nitrogen. In general, the polymer is composed of about 10^5~10^6 numbers monomer to compose a large polymer bond, shown in Fig. 2-2-c.

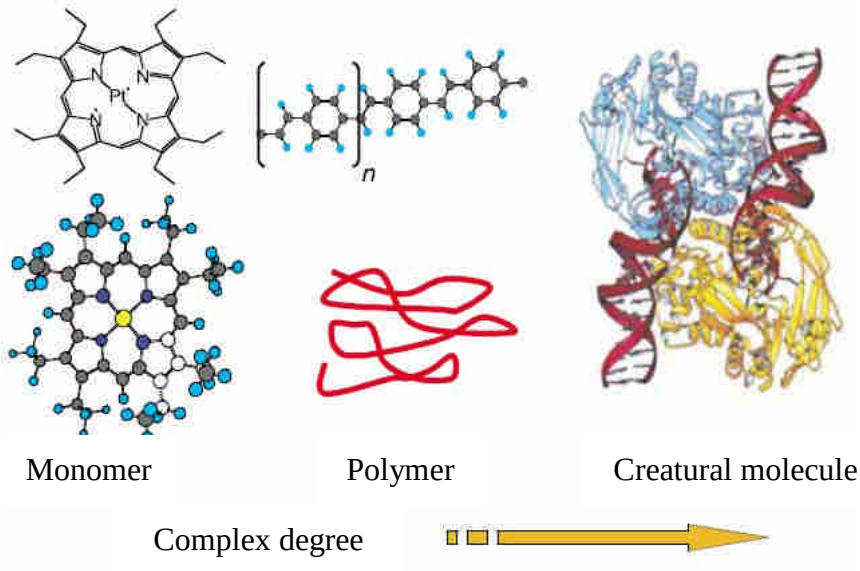

Fig. 2-2-c The complex degree of the organic materials

The carbon element on the back-bond for conjugate polymer has the unsaturated bond so that composes an alternate bonding with single and double bond. The conjugate single-bond and double-bond is called the conjugate bonding. The simplest conjugate polymer is polyacetylene as Fig. 2-2-d.

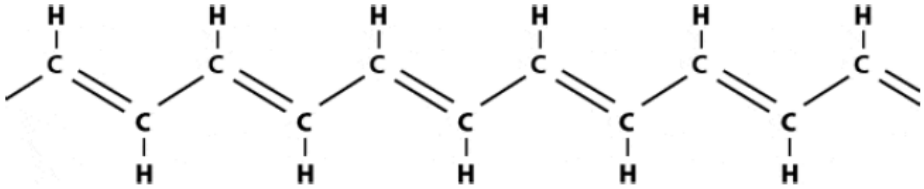

Fig. 2-2-d Polymer molecular structure of polyacetylene

From the electronic orbital theory, there is an electron on the sp^2 orbit among the carbon atom that combines with the hydrogen atom, and the other two sp^2 orbits combine with another sp^2 orbit for the nearest carbon atoms that become the single σ-bond. Nevertheless, the σ-bond is not beneficial for electronic transmission because that has the properties with the large band gap, the narrow energy width, and the small molecular orbit. In addition, the vertical orbit of the sp^2 plane overlaps with the other orbit for the nearest carbon atoms, attributed to a delocalized π-band. That enables electrons to move on the polymer chains that induces the electronic conduction. Therefore, the conjugate polymer is called the conducting polymer. The special property of the conjugate polymer is the electronic conduction that could be controlled by doping to a conductor or an insulator as Fig. 2-2-e.

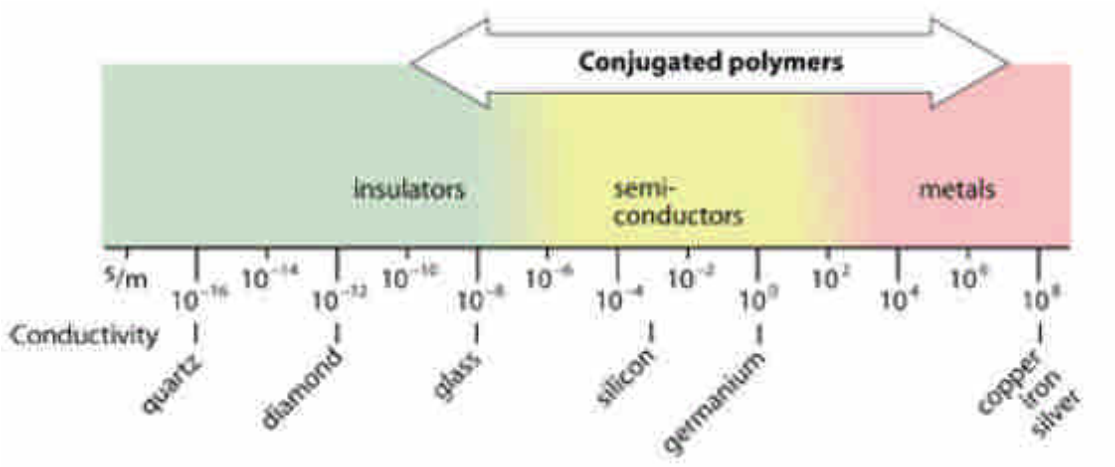

Fig. 2-2-e The electronic conduction region of the conjugate polymer by doping

Chapter 3 Method

3.1 Experimental system

3.1.1 Working principle of blade coating

Fig. 3-1-a shows the schematic working principle of blade coating. The thickness of the wet polymer film is defined by the gap. The polymer dry film thickness is tuned by the polymer concentration in solution and the gap of the blade coater. The polymer wet film is deposited by dragging the blade coater at a certain speed about 15 cm/s.

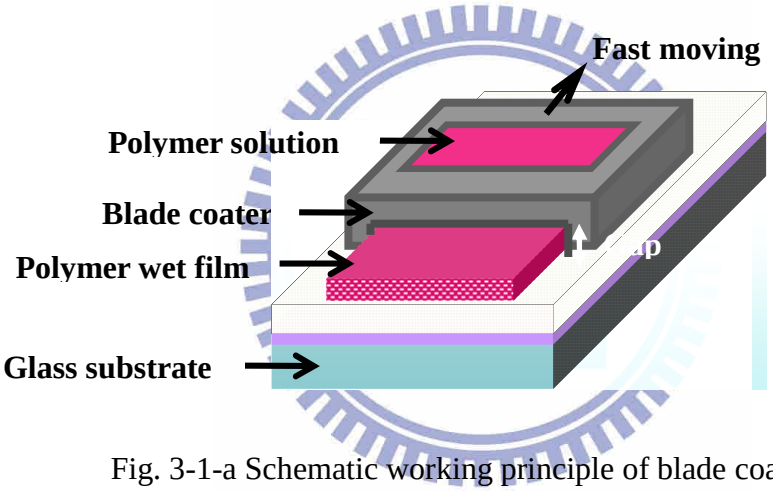

Fig. 3-1-a Schematic working principle of blade coating

3.1.2 Device structures

The development of the organic solar cells is to develop multilayer device structure and the bulk hetero-junction devices. Considering all of the development processes, the main idea is to increase the separation region for excitons. In this study, we used the bulk hetero-junction structure with single layer. The bulk hetero-junction device is made by the P3HT donor and PCBM acceptor blending. The device structure is designed for ITO/PEDOT:PSS/P3HT:PCBM/Ca/Al shown in Fig. 3-1-b (a). ITO is the anode and PEDOT:PSS (Baytron PVP AI 4083) is the hole transport layer. The active layer is used the

P3HT and PCBM blending in organic solvent, and the cathode Ca/Al is used. The energy band for the structure is shown in Fig. 3-1-b (b).

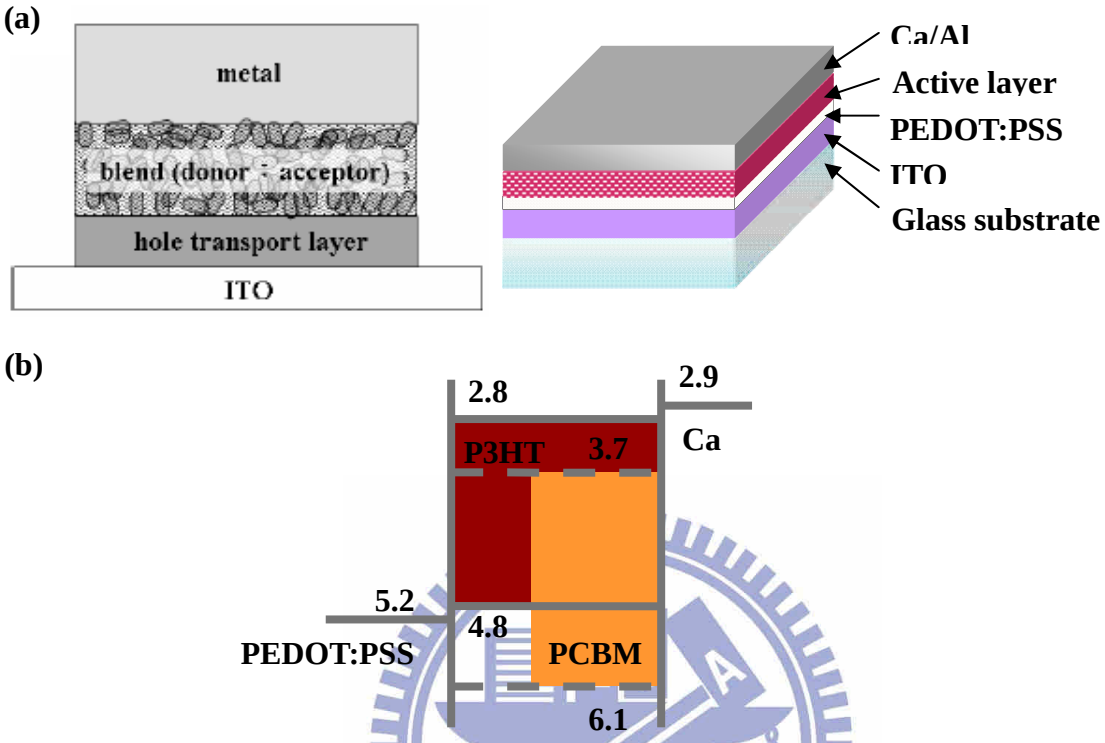

Fig. 3-1-b Single layer structure of bulk hetero- junction cells (a) device structure (b) energy band

3.1.3 Material introduction

A. Hole transport layer

For Fig. 3-1-c, the hole transport layer is poly-(3,4-ethylenedioxythiophene): poly-(styrenesulfonate) (PEDOT:PSS) with LUMO of 3.6 eV and HOMO of 5.2 eV. The PEDOT is an aqueous solution of polymer. It is not only for the hole transport but also for flattening the ITO substrate. In addition, the PEDOT:PSS layer conforms with the advantage of the light transmission. According to the different ratio between PEDOT and PSS has the different types and resistance. As the type of AI4083 is 1:6 ratio for PEDOT:PSS and the volume resistivity is about 500-5000 ohm-cm.

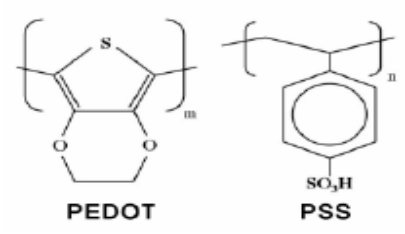

Fig. 3-1-c Molecular structures of PEDOT and PSS

B. Active layer

The active layer is used the P3HT and PCBM blending in organic solvent. The poly(3-hexylthiophene) (P3HT) with LUMO of 2.8 eV and LUMO of 4.8 eV is a common donor of polymer material that with the absorption wavelength among 500nm~600nm. In general, the electron mobility (μ_e= 10^{-4}~10^{-9} cm^2/V-s) is lower than the hole mobility (μ_h= 10^{-1}~10^{-7} cm^2/V-s) for polymers. Therefore the better donor material is chosen with the higher hole mobility. P3HT is a better hole mobility among the conjugate polymer. It had been measured the hole mobility about 10^{-1} cm^2/V-s [33]. Besides, the (6,6)-phenyl-C61-butyric acid methyl ester (PCBM) with LUMO of 3.8 eV and HOMO of 6.2 eV is a common acceptor of small molecular material. It is a derivative for C_{60} that has the higher electron transport ability and the absorption wavelength is about 350nm. But the PCBM could not be easily dissolved in organic solvents by itself that needs some other polymer material as guest to increase solubility.

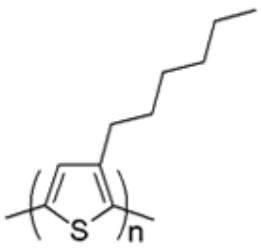

Fig. 3-1-d The monomer structure of P3HT

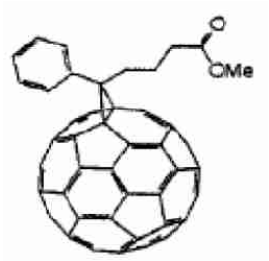

Fig. 3-1-e The molecule structure of PCBM

3.2 Experimental process and measurement

3.2.1 Deposition of the hole transport layer

The patterning ITO coated glass substrates were cleaned by ultrasonic treatment with organic solvent, detersive and deionizer water successively. After removing the smirch on the substrate, the cleaned substrates were baked on hot plate with 100 ℃ for several minute. Then ITO substrates are treated by UVO_3 with 20 minutes for the formation a hydrophilic surface. PEDOT:PSS (Baytron PVP AI 4083) film with the thickness about 40 nm as hole transport layer was spin coated in air and then baked at 200 ℃ for 15 minutes in nitrogenous glove box.

3.2.2 Deposition of the active layer

The blend of P3HT:PCBM with 1:1 ratio formulated 17 mg/ml respectively dissolved in toluene, chlorobenzene (CB), and dichlorobenzene (DCB). The solutions were heated at 60 ℃ for 12 hours at least. We first focus on solar cells with P3HT:PCBM blend dissolved in toluene. Device performances are compared for different coating methods including spin coating, blade coating, blade coating on a hot plate, as well as blade and spin coating. For the blade and spin coating the polymer wet film is deposited by blade coating which is followed by spinning until the dry film is formed.

Seven series of devices with six devices in each are made to study the different coating processes with different solvents statistically. Among them, five series are made with toluene solution to compare the coating processes, including spin coating (series A), blade coating (series B), blade coating on a hot plate at 60℃ (series C), as well as blade and spin coating (series D). In addition, the devices with the PEDOT:PSS layer by blade coating at 100℃ and P3HT:PCBM by blade and spin coating from toluene solution is made to study

the feasibility of bladed PEDOT:PSS layer (series G). The other two series made from two conventional high boiling point solvents, chlorobenzene (series E) and dichlorobenzene (series F), are compared with those from toluene by blade and spin coating. After coating all the P3HT:PCBM layers are annealed at 140℃ for 20 minutes in nitrogen.

The Ca(35nm)/Al(100nm) cathode was deposited by thermal evaporation. The active area of the device was 0.04 cm^2. All the devices were packaged in the glove box and measured in the ambient environment.

3.3 Measurement

3.3.1 Photovoltaic property

The PCE is measured by the solar simulator (PEC-L11, Peccell Technologies) under AM1.5G irradiation.

3.3.2 External quantum efficiency

The incident photon-to-electron conversion efficiency (IPCE) is measured by the spectral response measurement system (SR300, Optosolar GMBH).

3.3.3 Morphology

The morphology of P3HT:PCBM is monitored by atomic force microscope (AFM, Dimension 3100, Digital Instruments).

Chapter 4 Result and discussion

4.1 Device performance of bulk hetero-junction cells

Fig. 4-1-a shows the statistical results of the seven series of devices. Among the series based on toluene solution (series A, B, C, D, and G), the series of devices by blade coating have the higher efficiencies except the series with bladed the PEDOT:PSS layer. Because the V_{oc} are about the same, the high performances of series B, C, and D result from the high short circuit current density J_{sc} and fill factor. Among the series by blade and spin coating (series D, E, and F), the series of devices from toluene solution and dichlorobenzene have the higher performances. While the J_{sc} of series E and series F are about the same, the high performance of series F results from the relatively high fill factor. For further discussion, the best devices in each series are chosen to show the advanced device properties.

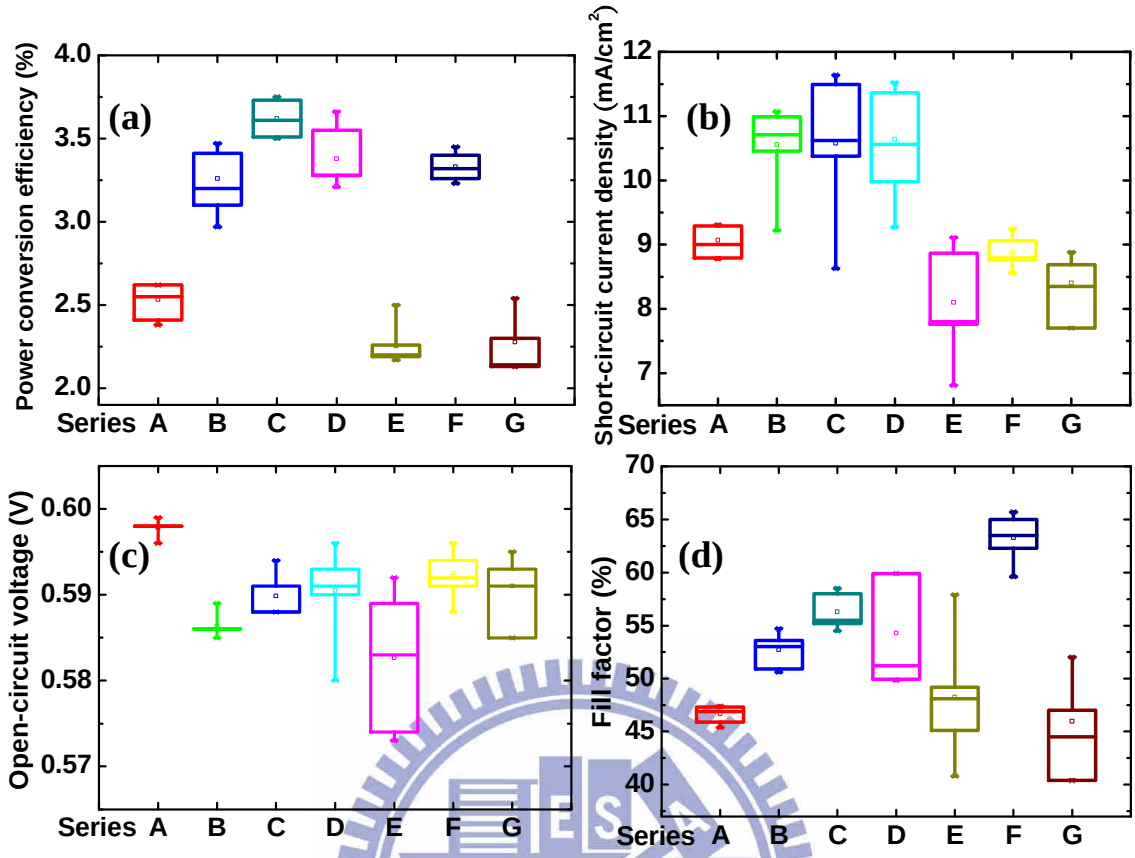

Fig. 4-1-a Statistical results of the seven series of devices, (a) the PCE, (b) the J_{sc}, (c) the V_{oc}, and (d) the fill factor. The horizontal lines in the box denote the 25th, 50th, and 75th percentile values. The error bars denote the 5th and 95 percentile values. The open square inside the box denotes the mean value.

Fig. 4-1-b (a) shows the current density-voltage (J-V) curves of five devices in toluene solution made by different active layer coating processes. The short circuit currents J_{sc} made by blade coating (device B, C and D) are larger than that of the device made by conventional spin coating (device A). Using blade coating the J_{sc} increases from 9.3 mA/cm^2 with spin coating to 11.5 mA/cm^2. The fill factor rises from 47% to 55% and the V_{oc} remains the same. The efficiency, which is proportional to J_{sc}, V_{oc}, and fill factor as a whole, is improved from 2.6% (device A) by spin coating to 3.8% (device C) by blade coating on a hot plate.

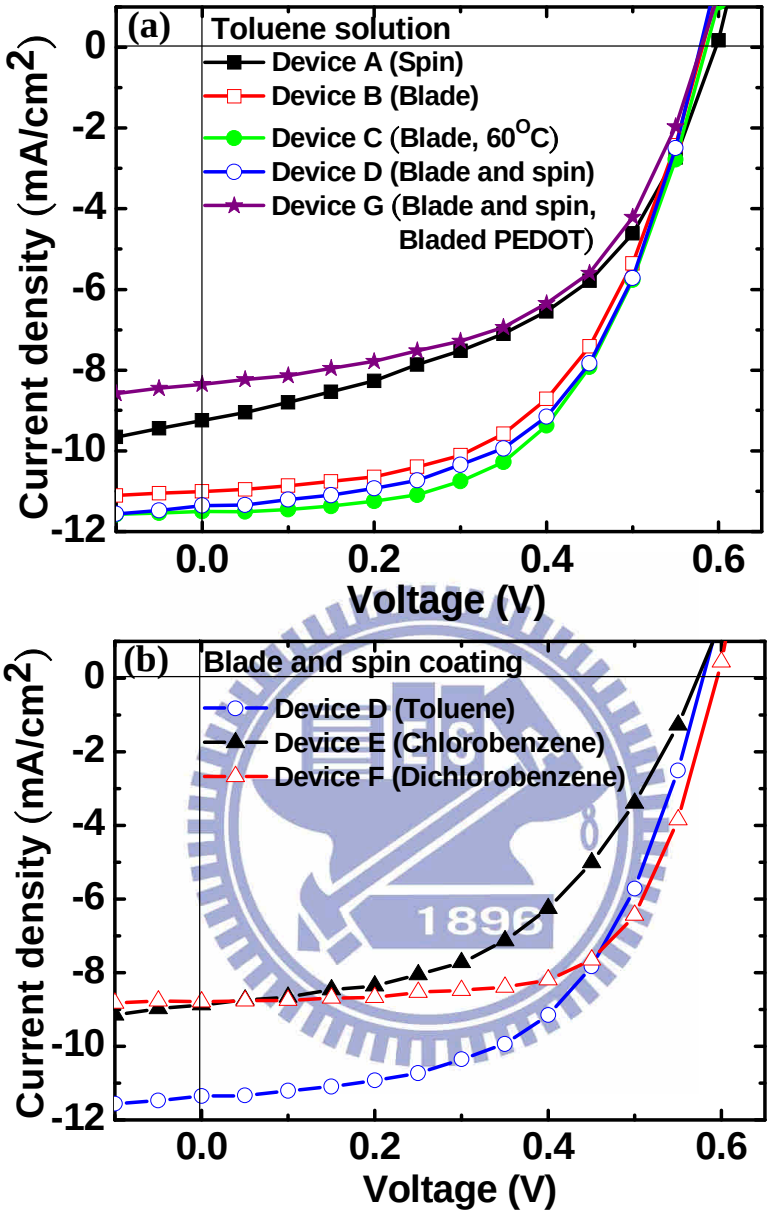

Fig. 4-1-b Current density-voltage (J-V) relations of the devices. (a) Devices made by spin coating (device A, solid square), blade coating (device B, empty square), blade coating at 60 ℃ (device C, solid circle), and blade and spin coating (device D, empty circle) in toluene solution, blade and spin coating with bladed PEDOT:PSS (device G, solid star) (b) Devices made by blade and spin coating in toluene solution (device D, empty circle), chlorobenzene solution (device E, solid triangle), and dichlorobenzene solution (device F, empty triangle)

It is believed that in order to get a high efficiency in bulk hetero-junction polymer solar cell the microscopic morphology of the active layer needs to be well controlled to achieve an ordered structure by certain annealing processes such as slow solvent evaporation1 and postproduction heat treatment [22]. Such annealing promotes molecular self-organization and makes the polymer chains more ordered in its domains. In spin coating for low boiling point solvents such as toluene (110 ℃), high volatility leads to the fast drying of the active layer and may limit the self-assembly as well as the PCE. However, the polymer films made by blade coating could be more ordered than those by spin coating due to the fact that the polymer chains are relatively free to move in the absence of centrifugal force. Therefore even without the slow drying process the donors and acceptors quickly self-assemble into the desired ordered and interpenetrating morphology during the blade coating process. We speculate that the quick assembly occurs at the beginning of the blade coating because the device made by blade and spin coating (device D) shows high efficiency as well. Interestingly, device B, C, and D have different film thickness but similar performances. High efficiency is maintained for device B with 412 nm thickness probably because pure blade coating with neither heating nor spinning give the highest freedom to chain motions and the most ordered morphology. In short, the blade coating method allows ordered polymer morphology in a fast drying solution like toluene. In addition, the result of the device with the bladed PEDOT:PSS and blade and spin coated P3HT:PCBM layer is also shown in Fig. 4-1-b (a). The efficiency of device G is 2.5% with J_{sc} of 8.35 mA/cm^2, V_{oc} of 0.59 V, and fill factor of 52%. The relative low performance of device G results from the thick PEDOT:PSS film (120 nm), which causes high series resistance. It is difficult for us to reduce the PEDOT:PSS film thickness now because we use the PEDOT:PSS solution from H. C. Stark without any further dilution. The concentration needs to be lowered without sacrificing the conductivity to get the normal film thickness (40 nm). More experiments need to be done to optimize the PEDOT:PSS layers by blade coating. Nevertheless, such

device shows the feasibility of all blade coated devices with very low cost and high throughput in mass production.

Now we turn to different solvent systems. Two devices are made by conventional high boiling points solvents chlorobenzene (device E) and dichlorobenzene (device F). Fig. 4-1-b (b) shows the results of the devices by the fast-drying blade and spin process with different solvents. There is no slow solvent evaporation in the fabrication process. The power conversion efficiencies are 2.5% in the device from chlorobenzene solution (device E) and 3.5% in that from dichlorobenzene solution (device F). The J_{sc} are both about 8.8 mA/cm^2, which is significantly smaller than J_{sc} of 11.4 mA/cm^2 in device D from toluene. Interestingly high boiling point solvents give higher J_{sc} for spin coating but smaller J_sc for blade coating. There are probably more P3HT/PCBM interfaces in toluene solution than those in chlorobenzene and dichlorobenzene solutions, resulting in more efficient exciton dissociation. It is remarkable that the fill factor of dichlorobenzene solution is 66 %, much higher than 55 % for toluene and 49 % for chlorobenzene. Dichlorobenzene has the highest boiling point among the three solvents. The highest fill factor in dichlorobenzene solution may result from the highest carrier mobility due to the enhanced self-assembly of P3HT taking place during the relatively slow drying in spinning. The device performances are summarized in Table 1.

Table 4-1 Performance of bulk hetero-junction solar cells in this work.

Label	J_{sc} (mA/cm^2)	V_{oc} (V)	Fill factor (%)	PCE (%)	Thickness (nm)
A. (Toluene)Spin	9.25	0.59	47	2.6	223
B. (Toluene)Blade	11.07	0.59	53	3.5	412
C. (Toluene)Blade at 60℃	11.49	0.59	55	3.8	304
D. (Toluene)Blade and spin	11.36	0.58	55	3.7	245
E. (Chlorobenzene)Blade and spin	8.87	0.57	49	2.5	345
F. (Dichlorobenzene)Blade and spin	8.79	0.60	66	3.5	242
G. (Toluene)Blade and spin with bladed PEDOT:PSS (120 nm)	8.35	0.59	52	2.5	245

The AFM images of the devices are shown in Fig. 4-1-c. The root-mean-square (RMS) roughness are 2.3 nm for device A, 15.1 nm for device B, 4.9 nm for device C, 2.8 nm for device D, 1.9 nm for device E, and 5.8 nm for device F. The different root-mean-square values are attributed to the different fabrication processes with different solvents. We think that the devices with high efficiency (device B, C, D, and F) have stronger self-organization than those with low efficiency (device A and E). Higher surface roughness corresponds to higher degree of self-organization [34]. However, there is no clear evidence for the correlation between self-organization and device efficiency. Nevertheless, we speculate that device B by blade coating shows clear self-organization, implying ordered structures within each component. Therefore, the carrier mobility is high and the power conversion efficiency is high as well even with a thick film of 412 nm. The clear self-organizations in device C and device F also could be seen due to their relative high roughness. Interestingly, the roughness of device D by blade and spin coating is just slightly higher than that of device A only by spin coating, but the efficiency of device D is still much higher. This may be due to the ordered structure occurred at the beginning of blade coating, combined with thicker film thickness by blade coating. As for the low efficiency devices such as device A and device E, the films are relatively smooth. The images show that the self-organization could be

achieved within the short drying time by blade coating.

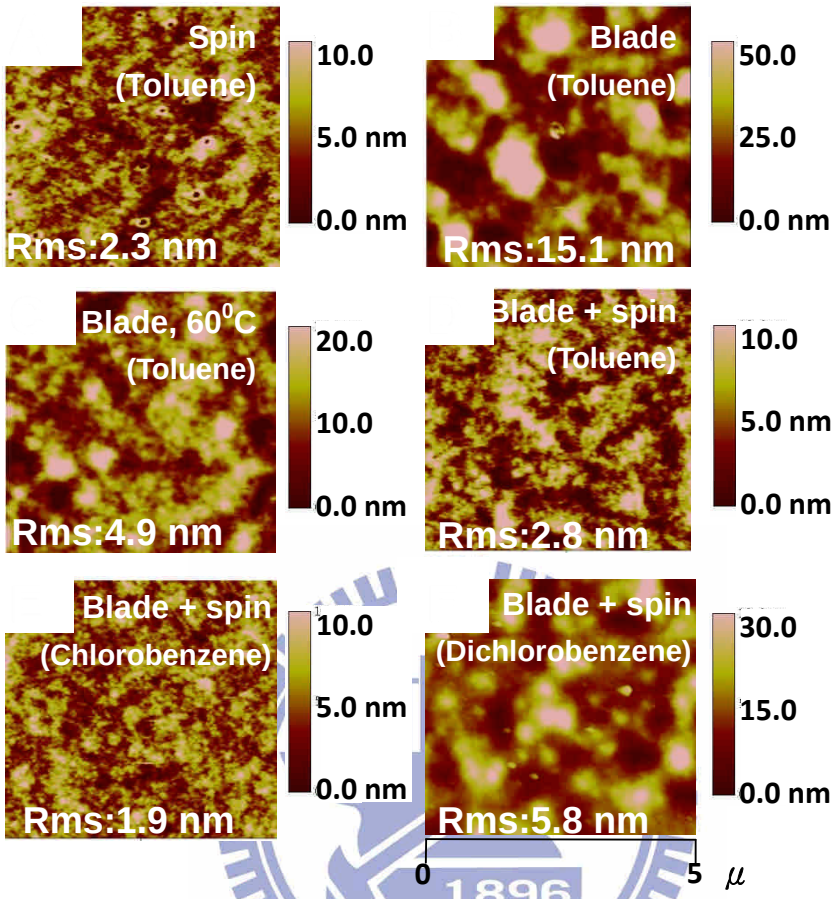

Fig. 4-1-c AFM images of the devices in this work. P3HT:PCBM thin film made by (a)spin coating, (b)blade coating, (c)blade coating at 60° C, (d)blade and spin coating, (e) blade and spin coating in chlorobenzene solution, (f) blade and spin coating in dichlorobenzene solution. The P3HT:PCBM films in (a) to (d) are made in toluene solution.

Fig. 4-1-d (a) shows the absorption spectra of the P3HT and PCBM blend films deposited by different methods and solutions. The IPCE for all devices are shown in Fig. 4-1-d (b). Despite of the different morphologies there is no significant variations among the absorption spectra. So the differences in the device performances must come from the exciton dissociation and carrier transport processes. The IPCE values appear similar in all the devices except that of device G and show slightly difference at about 600 nm. However, the J_{sc} values show much difference among the devices. In principle the measured J_{sc} should

be proportional to the product of the IPCE and the illuminating spectrum, integrated over all wavelengths. We may attribute the inconsistency between IPCE and J_{sc} values to the different spectral-mismatch factors of the different light sources [26].

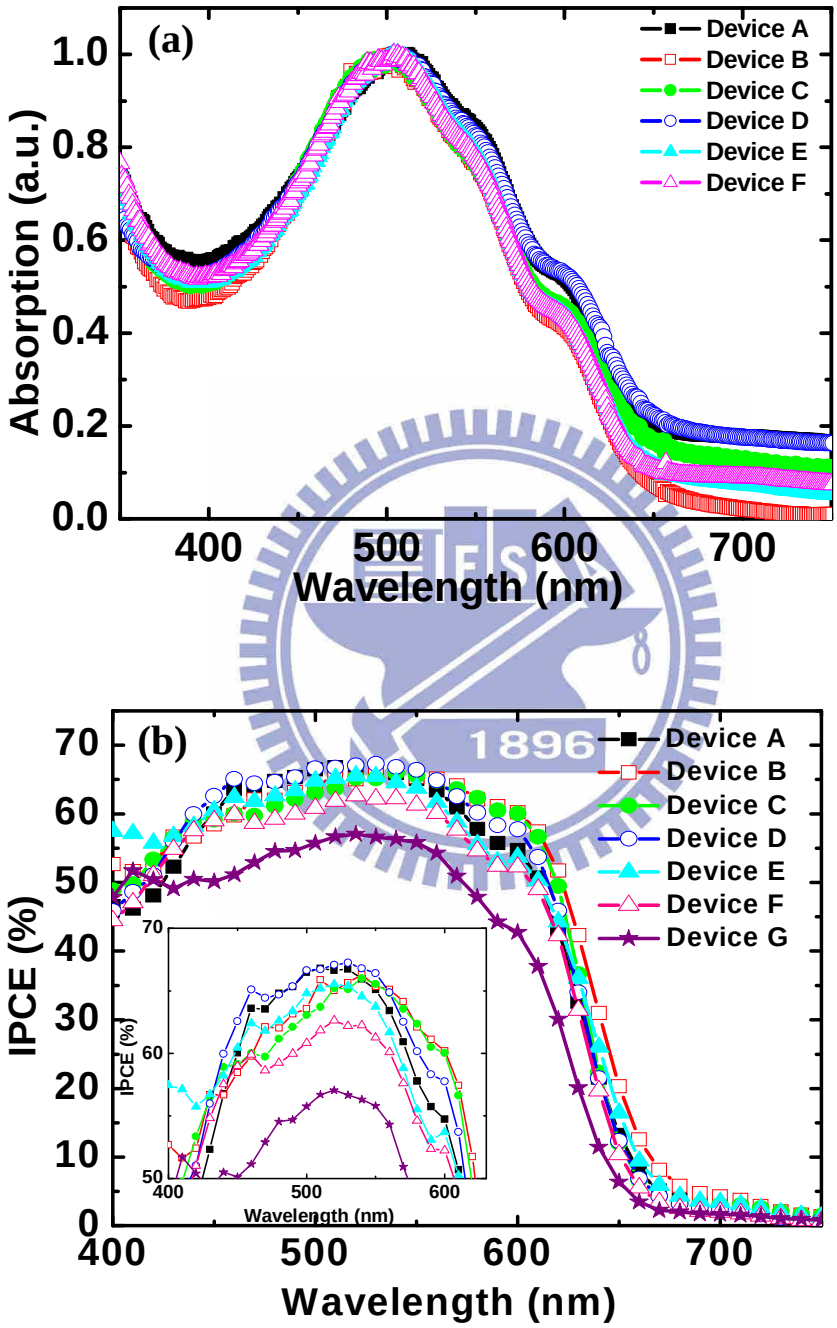

Fig. 4-1-d (a) The absorption spectra of devices. (b) The incident photon to current efficiency (IPCE) in this work

4.2 Roughness of net P3HT and PCBM film

Fig. 4-2-a and Fig. 4-2-b show the morphology of thin film for net P3HT and pure PCBM with the same experiment conditions between Fig. 4-1-c like the fabrication processes and the solvents for each components. It is easy to discover the difference between the properties of grown net P3HT and PCBM thin film. All of the net P3HT films have the root-mean-square (RMS) roughness with about 15±3 nm that tends to form the aggregation between P3HT polymers. However, there seems not be clear division among the different fabrication processes and different organic solvents. We turn to observe that the roughness of PCBM, it is evident that the film property is greatly different between net P3HT films. The PCBM films have the tendency to form the crystals because the roughness becomes much higher. A lower RMS case (Fig. 4-2-b, sample F) among the net PCBM films that may due to the experimental variation such as the film thickness or the man-made effect during blade coating process.

The films of P3HT and PCBM blending have the lowest roughness among three types that can be attributed to mutually restrain the effect on aggregation for P3HT and the crystal for PCBM.

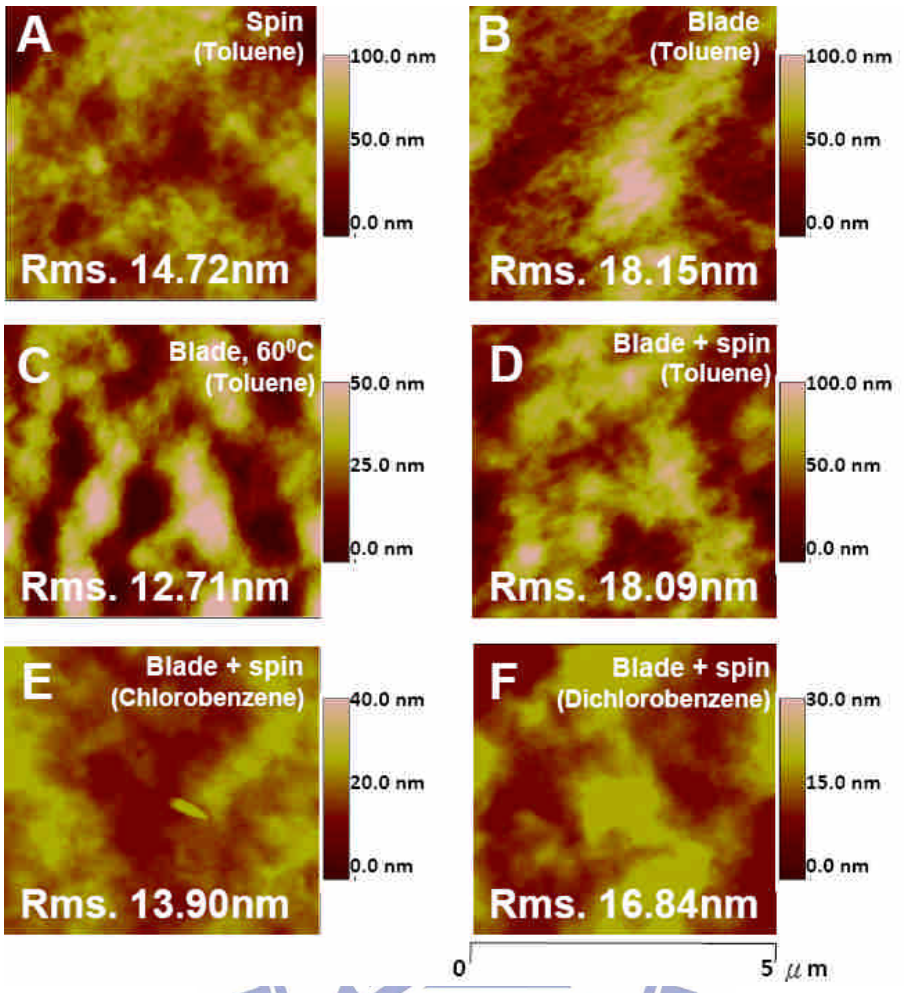

Fig. 4-2-a AFM images of net P3HT thin film made by (a)spin coating, (b)blade coating, (c)blade coating at 60° C, (d)blade and spin coating, (e) blade and spin coating in chlorobenzene solution, (f) blade and spin coating in dichlorobenzene solution. The P3HT films in (a) to (d) are made in toluene solution.

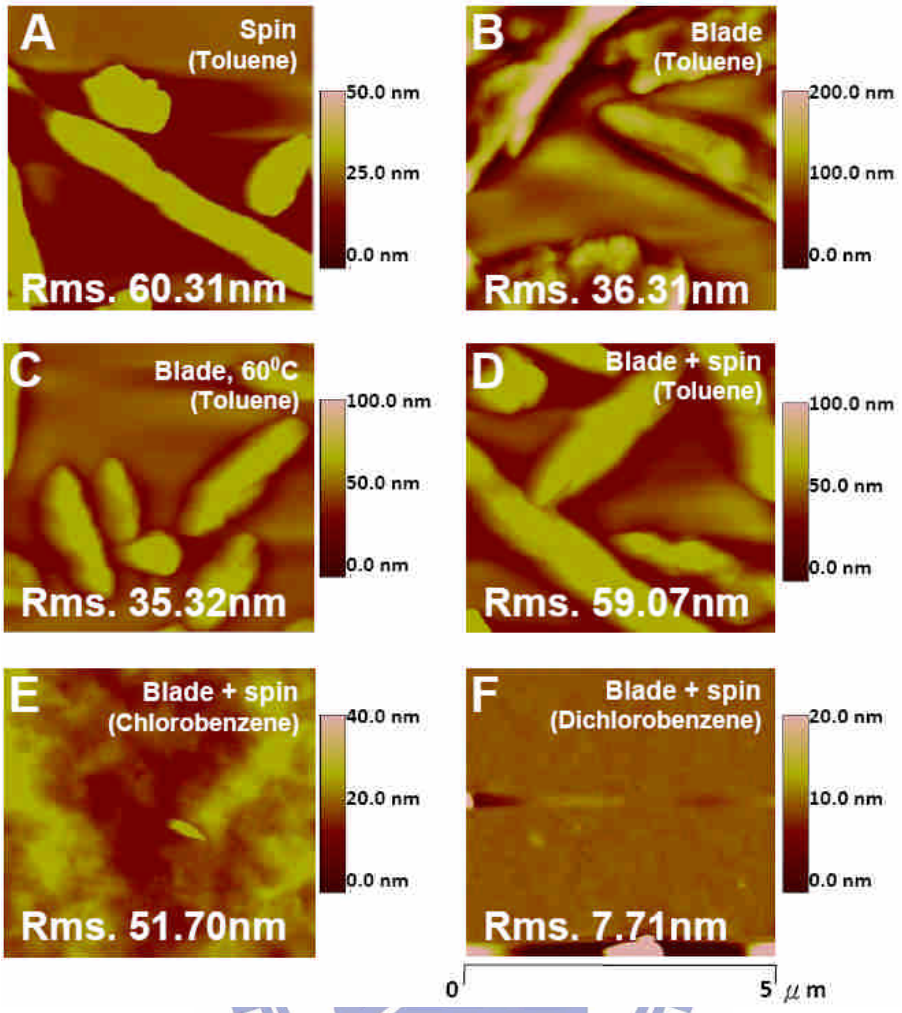

Fig. 4-2-b AFM images of the PCBM thin film made by (a)spin coating, (b)blade coating, (c)blade coating at 60° C, (d)blade and spin coating, (e) blade and spin coating in chlorobenzene solution, (f) blade and spin coating in dichlorobenzene solution. The PCBM films in (a) to (d) are made in toluene solution.

Table 4-2 The roughness of P3HT:PCBM, net P3HT, and net PCBM films

Label	**RMS (nm)**		
	P3HT:PCBM	**P3HT**	**PCBM**
A. (Toluene)Spin	2.3	14.7	60.3
B. (Toluene)Blade	15.1	18.2	36.31
C. (Toluene)Blade at 60℃	4.9	12.7	35.3
D. (Toluene)Blade and spin	2.8	18.1	59.1
E. (Chlorobenzene)Blade and spin	1.9	13.9	51.7
F. (Dichlorobenzene)Blade and spin	5.8	16.8	7.71

Chapter 5 Conclusion

In conclusion we develop the blade coating method to fabricate bulk hetero-junction polymer solar cells with decent power conversion efficiency of 3.8 %. The active layer is deposited from toluene solution, which is less toxic than the chlorobenzene and dichlorobenzene solution optimized for spin coating. In sharp contrast to spin coating there is almost no material waste in blade coating. Moreover, this method can be easily scaled up to large sizes as meters and can be applied in a future roll-to-roll fashion for mass production.

Part 2 Multilayer polymer photo-detectors

Chapter 6 Introduction of polymer photo-detectors

6.1 Background of research

6.1.1 Introduction of polymer proximity sensors

Proximity sensor is the device which can sense the approaching objects without contact. According to the different materials, it could be classified as the inorganic proximity sensor and the polymer proximity sensor. Today the inorganic proximity sensor has been well developed and applied to the mechanical robot in automatic products. However the fabrication of the inorganic proximity sensor needs the high fabrication temperature, complex processes, the inflexibility property, and the high cost. Besides, there are some problems of inorganic proximity sensor such as the difficulty to scare up to the large-area size with high density sensing array. On the contrary, the polymer proximity sensor has the advantages like the low cost fabrication, easy fabrication processes from solution, large-area with high density array, and the potential of the flexibility. The polymer proximity sensors can be extensive applied in the robot skin that could increase the usage region such as in the safety, nursing, housework, and so on.

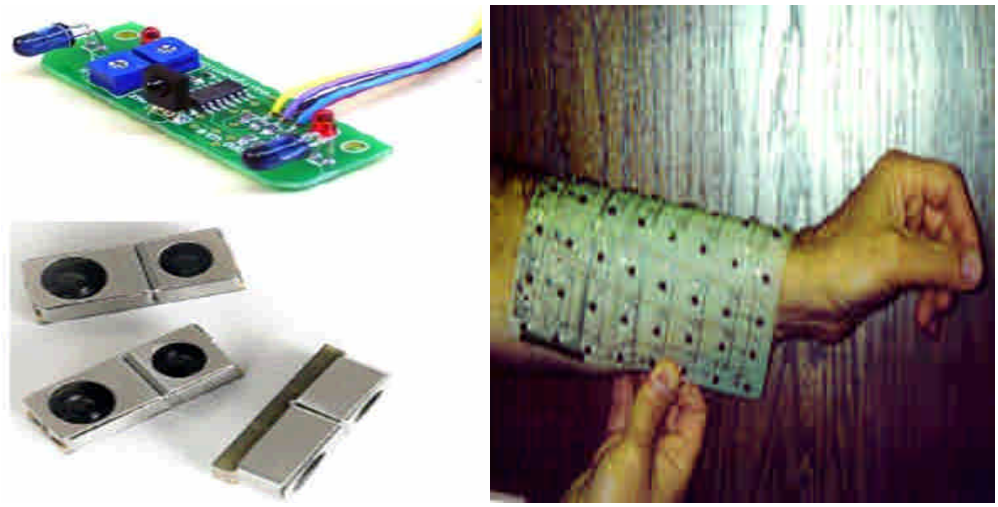

Fig. 6-1-a Inorganic proximity sensors

6.1.2 Development of polymer proximity sensors

The proximity sensor is made by a light-emitting diode as light source and a photo-detector as light receiver. In 1963 year, the first organic light-emitting diode (OLED) was made by anthracene crystal as emission layer material; it was a poor device performance [36]. Until 1987 year, Kodak used the Alq_3 as the emission layer to fabricate a green light OLED with the low operation voltage (below 10 volts). Until 1990 year, the polymer light-emitting diode (PLED) was developed by Friend Group in England. The PLED was made with poly(p-phenylene vinylene) (PPV) by spin coating [37]. Recently, the PLED is developed with quick speed for the high efficiency and high luminance.

The photo-detector has the same device structure as polymer bulk hetero-junction solar cell in this work. The difference between photo-detector and solar cell is the operating voltage. The photo-detector is operated under reverse biases. The reverse bias is applied to improve the carrier transport ability to increase the carrier collection by electrodes. The relative introduction of the polymer solar cell development is in the section 1-1-3.

6.1.3 Introduction of polymer photo-detectors

Fig. 6-1-b shows the proximity sensor device is composed by a light source PLED and a polymer photo-detector. The working principle of the proximity sensor is that the light is emitted from PLED, reflected by the approaching object surface, and then sensed by the photo-detector. In short, the photo-detectors transform the absorption photons to electrons, and the current change is detected to sense the distance between the objects.

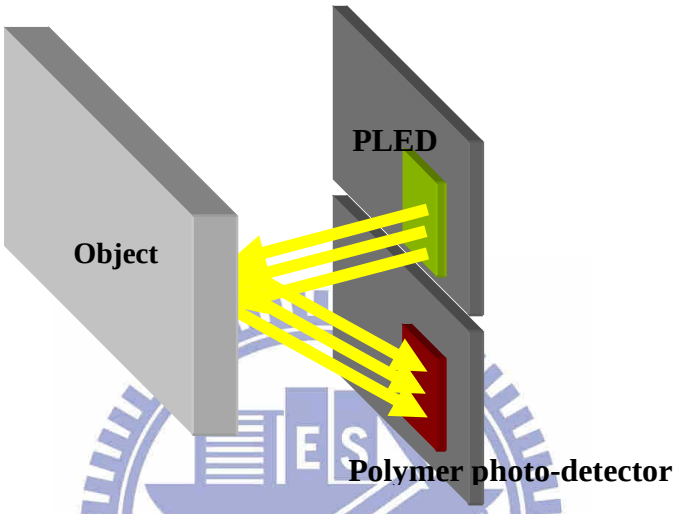

Fig. 6-1-b Schematic the working principle of polymer proximity sensor

The performance of the polymer photo-detector is relative with the current-voltage in the reverse biases shown in Fig. 6-1-c (a), which is different from the solar cell with a small forward bias shown in Fig. 6-1-c (b).

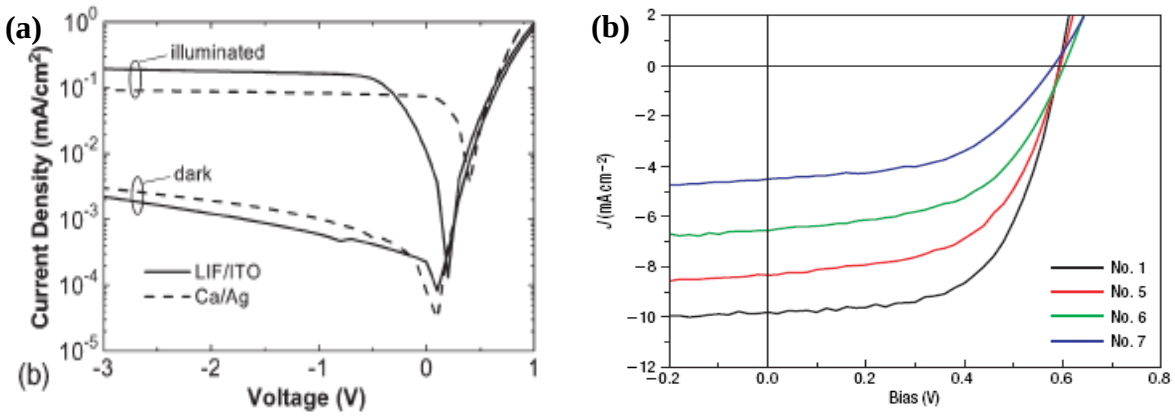

Fig. 6-1-c The current-voltage curves (a) photo-detector device with a reverse bias [38] (b) solar cell device with a positive bias [39]

6.2 Motivation of research

6.2.1 Problems of polymer photo-detectors

A good polymer proximity sensor should have good performance for the light source and the photo-detector. In this study, we focus on the high sensitivity photo-detector that implies the device with high photocurrent generation and low dark currents. The photocurrent generation is decided by materials, fabrication processes of active layer, and the microscopic morphology between the components. Otherwise the dark current comes from the operation in the reverse bias. Apply a reverse bias in order to increase carrier transport ability of the active layer to increase the efficiency of the carrier collection by electrodes. But that would induce the serious dark carrier injection to form the dark current at the same time. The so-called dark carrier is the electrons injected from the anode and the holes injected from the cathode as well, shown in Fig. 6-2-a. The dark carrier transmissions direct is opposite to the photocurrent, which would reduce the photo-detector sensitivity. In order to improve the sensitivity, the dark current need to be reduces because the measurement current is the total current of photocurrent and dark current.

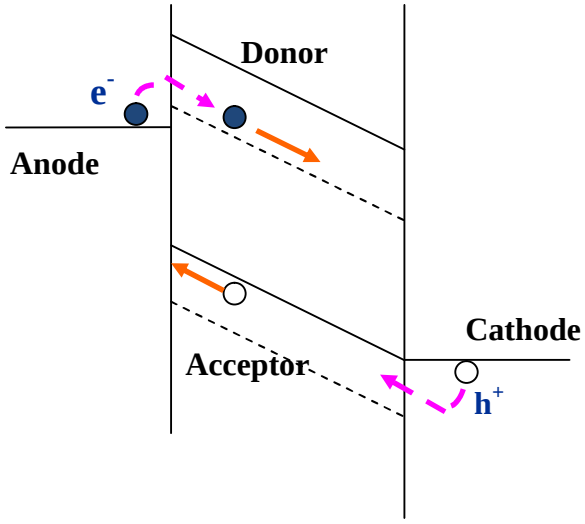

Fig. 6-2-a The origin of dark current

6.2.2 Multilayer structures

The multilayer structure is designed to solve the problem of high dark current by introducing the carrier blocking layers to avoid dark carrier injections. The blocking layers are designed as electron blocking layer (EBL) and hole blocking layer (HBL). Fig. 6-2-b shows the energy band diagram. The additional EBL between anode and active layer could form a barrier to avoid the electron injection from anode. The other side is HBL between active layer and cathode to avoid the hole injection from cathode.

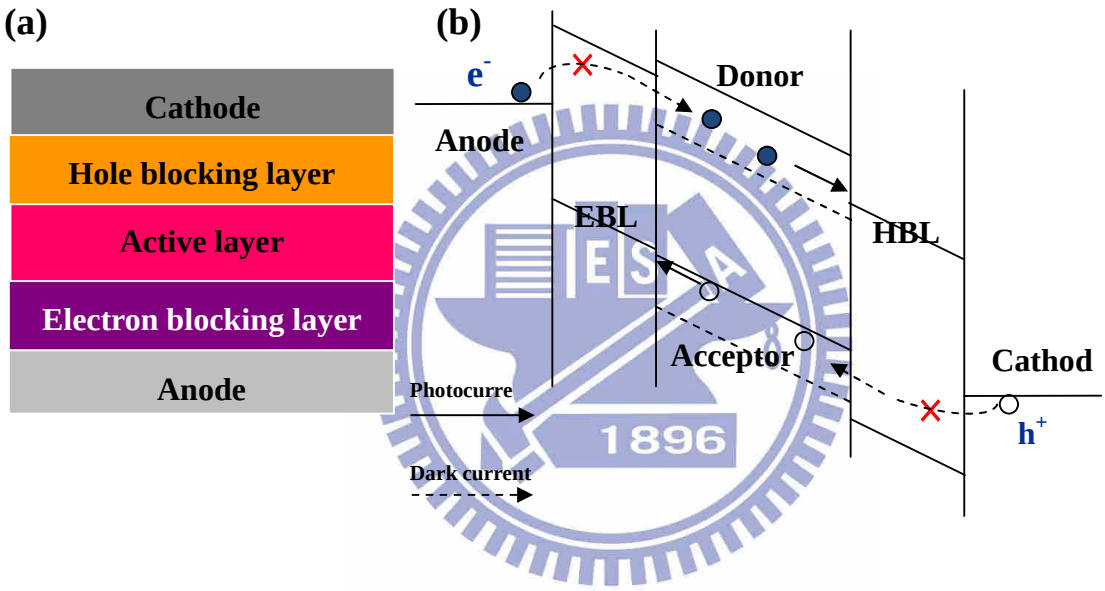

Fig. 6-2-b Multilayer structure of photo-detector to reduce the dark carrier injection (a) device structure (b) energy band

The multilayer structure is not easy to achieve by solution process because of there is a serious dissolution problem between polymer layers. In general, multilayer devices can be achieved by liquid buffer layer (BL) [40] and polymer transfer printing [41]. Another problem is the small molecule could not be deposited directly by solution processes for one component material generally because small molecules do not have side-chains or main-chains to form a thin film as Fig. 6-2-c

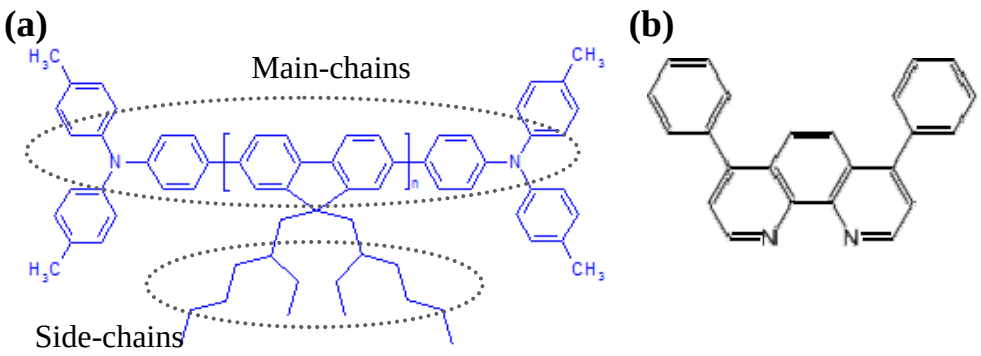

Fig. 6-2-c Chemical structure of (a) polymer (polyfluorene) (b) small molecule (BPhen)

6.2.3 Multilayer structures by Blade coating

The multilayer fabrication process by blade coating is shown in Fig. 6-2-d. Initially we deposit the first polymer thin film by blade coating. When fabricating the second polymer film, a heater is needed for multilayer process to expel the solvent of the second polymer solution. So the second film is formed by solution but quickly dried before dissolving the first polymer layer. All of the fabrication time of second polymer film is under 5 seconds from the deposition to the dried film. Here we has verified that the blade coating to fabricate multilayer PLED without dissolution between polymer layers shown in Fig. 6-2-e.

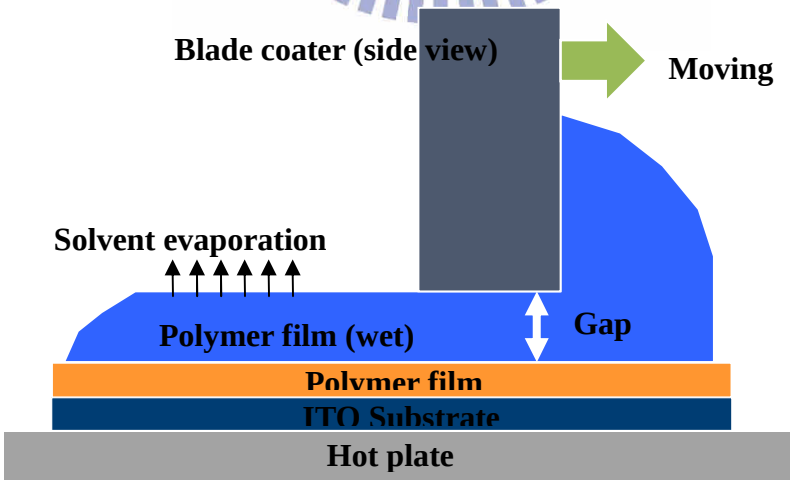

Fig. 6-2-d Schematic the working principle of blade coating

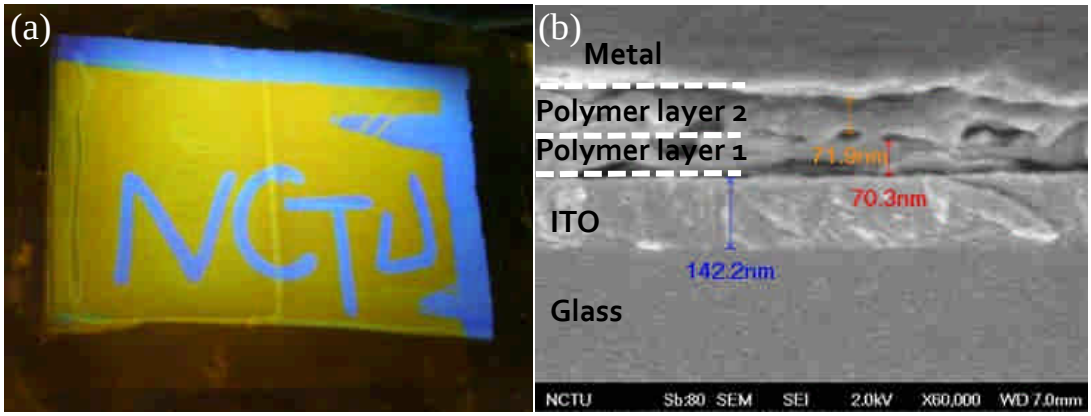

Fig. 6-2-e Double layer structure with no dissolution by blade coating for (a) PLED device (b) SEM [42]

6.3 Thesis frameworks for part 2

Chapter 6 Introduction

Introduced the background, motivation, and purposes of research

Chapter 7 Method

Introduced the experimental processes and materials

Chapter 8 Result

Discussed the experimental result

Chapter 9 Conclusion

Summary the important result of photo-detector research

Chapter 7 Method

7.1 Material introduction

Hole blocking layer

The hole blocking layer is the small molecular material such as PCBM and BPhen. The PCBM is also the acceptor material in active layer illustrated in section 3-1-3. The small molecular BPhen is usually applied to be the electron transport layer in OLED. BPhen with LUMO of 3.0 eV and HOMO of 6.2 eV is close to the band gap of PCBM, the molecular structure is shown in Fig. 7-1-a.

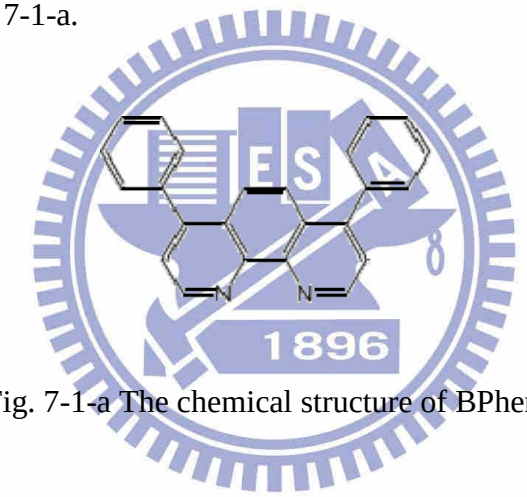

Fig. 7-1-a The chemical structure of BPhen

7.2 Experimental processes

The device fabrication processes of polymer photo-detector is similar to polymer solar cell, except the active layer with multilayer for photo-detector as the second step of Fig. 7-2-a. About the other steps of fabrication processes are referred the section 3-2.

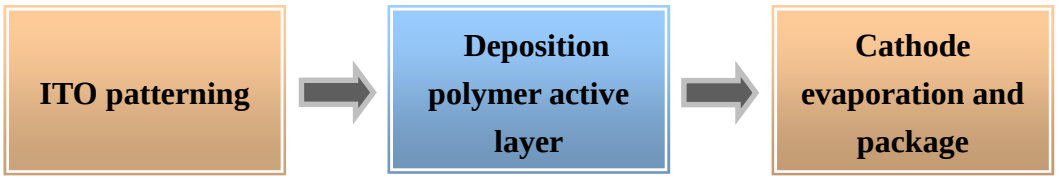

Fig. 7-2-a Fabrication processes of the polymer photo-detectors

7.2.1 Solution preparation

A. Electron blocking layer

The polymer P3HT with 0.5wt% in toluene, the solution was stirred on the hot plate with the 60℃ for 6 hours.

B. Active layer

The blend of P3HT:PCBM with 1:1 ratio formulate 17 mg/ml respectively dissolved in toluene, the solution is mixed and stirred at 60℃ for 12 hours at least.

C. Hole blocking layer

The PCBM is dissolved in toluene with 0.85wt%. Bphen is dissolved in methanol with 0.5wt%.

7.2.2 Deposition of the active layer

After cleaning and hole transport layer depositing of ITO substrate, and then carry the devices to the glove box to deposit the polymer layer in the nitrogen. In this study, we design the device structures with the single layer, bilayer, and trilayer devices, the detail of the device conditions are shown in Table 7-1.

Table 7-1 The conditions of the multilayer devices		
EBL material	Device structures	
PCBM	Single layer	P3HT:PCBM(350nm)
	Bilayer	P3HT(11nm)/P3HT:PCBM(340nm)
		P3HT:PCBM(340nm)/PCBM(~50nm)
		P3HT(200nm) /PCBM(100nm)
	Trilayer	P3HT(11nm)/P3HT:PCBM(340nm)/PCBM(~50nm)
BPhen	Bilayer	P3HT:PCBM(340nm)/BPhen(~50nm)
	Trilayer	P3HT(11nm)/P3HT:PCBM(340nm)/BPhen(~50nm)

The P3HT layers are deposition by spin-rinsed [43] and no spin-rinsed processes. First electron blocking layer P3HT is deposited by blade and spin coating with thickness about 11 nm and annealed at 200 ℃ for 10 minutes. The speed of blade process is about 15 cm/s. For blade and spin coating, the polymer wet film is deposited by blade coating which is followed by spinning until the dry film is formed; the fabrication is beneficial to control the film thickness. One of the bilayer structures with P3HT/PCBM, the P3HT is made by the same steps except the gap for blade coater and the spin rate to form a 200 nm thickness. The active layer is the P3HT:PCBM layer with the thickness of 340 nm that is deposited by the blade and spin coating with heating blow under the spinning process. All of the time for deposition active layer to dry is fewer than 4 seconds in order to avoid the dissolution. Than the active layer is baked at 140 ℃ for 20 minutes and cool down naturally on the turned-off hotplate for 20 minutes. Finally the HBLs are deposited by PCBM or BPhen. The PCBM layer is blade coated at 120 ℃ with coating speed as possible as fast to grow a about 50nm thin film, then heating at 140 ℃ for 20 minutes. The other device with BPhen layer is deposited by blade and spin coating with thickness of 50nm, and annealed at 50 ℃ for 7 minutes in nitrogen. The active layer for devices is shown in Fig. 7-2-b.

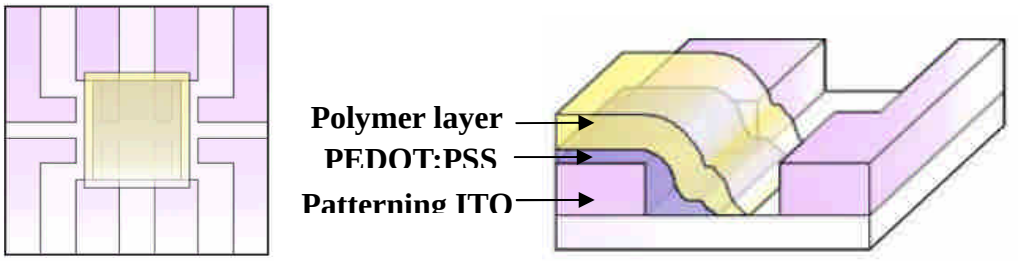

Fig. 7-2-b Fabrication of active layer

7.3 Measurement

7.3.1 Photovoltaic property

Fig 7-3-a shows the current-voltage relation is measured by the Keithley 2400. Using power supply to turn on the lamp source and the light through the grating could be chosen the measurement wavelength; finally the illumination is absorbed by the polymer photo-detectors. The Keithley 2400 connects with the photo-detector, and the amount of current is transmitted to a computer. When the light source turns on, the measurement of current-voltage relation is the photocurrent; otherwise the relation is the dark current in the dark room.

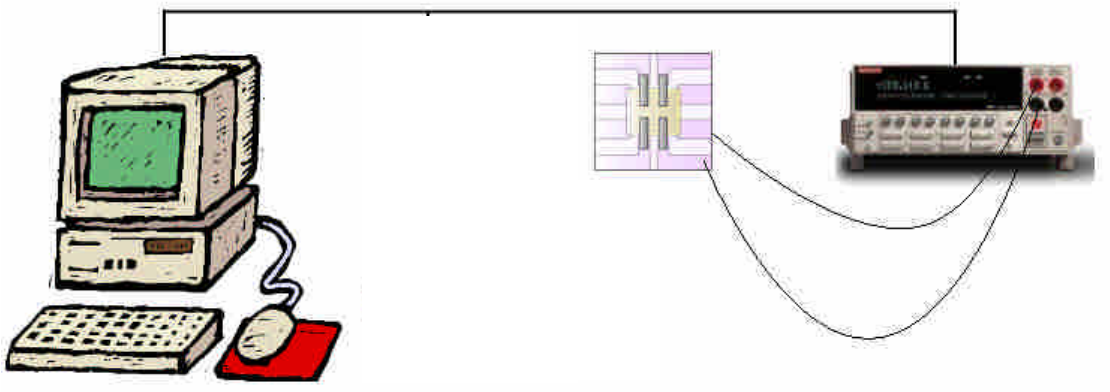

Fig. 7-3-a The device measurement of current-voltage relation

Chapter 8 Result and discussion

8.1 Single layer structures

8.1.1 P3HT diode with blade coating and spin coating

Fabrication of P3HT diodes has the same film thickness with photo-detector in order to understand the reduced limit of dark current. Comparison with different fabrication processes between spin coating and blade and spin coating is shown in Fig. 8-1-a and Fig. 8-1-b. As can be seen, the J-V characteristics have different tendency in the reverse bias. The current for spin coated device has the linear tendency change with the voltage, and the device for blade coating has the gentle change of current. The blade and spin coated device has the lower dark current performance with current density from 1.1×10^{-4} mA/cm^2 at -3V to 2.1×10^{-4} mA/cm^2 at -5V with the current change about 2 times. Otherwise the spin coated device has a quick change with current density from 1.5×10^{-4} mA/cm^2 at -3V to 5.3×10^{-4} mA/cm^2 at -5 V with current change over 3.5 times. The difference may due to the blade and spin coating could grow the smooth polymer film for the P3HT chains to become ordered arrangement during the blade coating that is beneficial for the carrier transport.

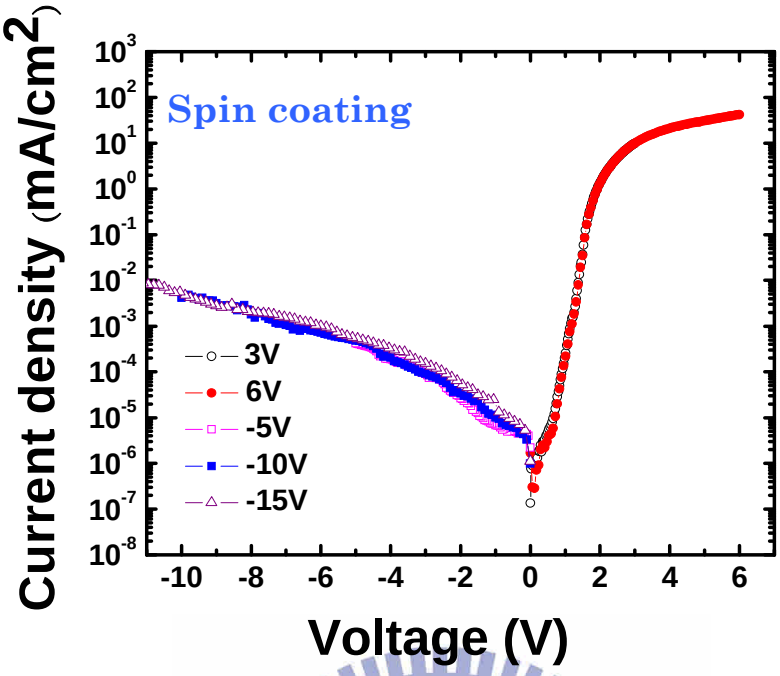

Fig. 8-1-a The J-V characteristics for P3HT diode by spin coating

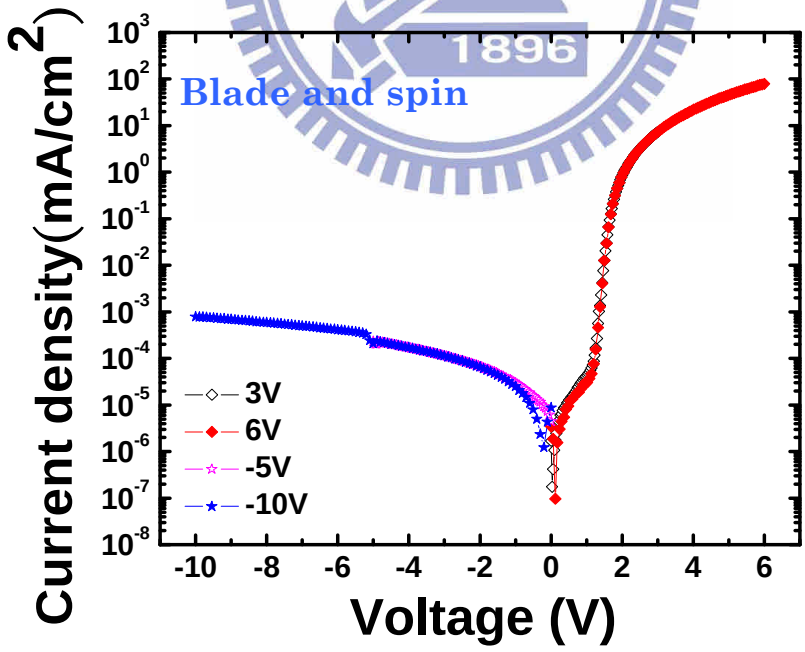

Fig. 8-1-b The J-V characteristics for P3HT diode by blade and spin coating

8.1.2 Single layer photo-detector by blade coating and spin coating

The dark currents for single layer photo-detectors show the different property between spin coated and blade and spin coated devices. As can be seen, the device by blade and spin coating has the clearly dark current tenfold lower than the spin coated device in the operating voltage during -3V to -5V. The remarkable difference may be attributed to the ordered chains by blade coated process that seems to be the most important influence on the self-organization between two components of P3HT and PCBM.

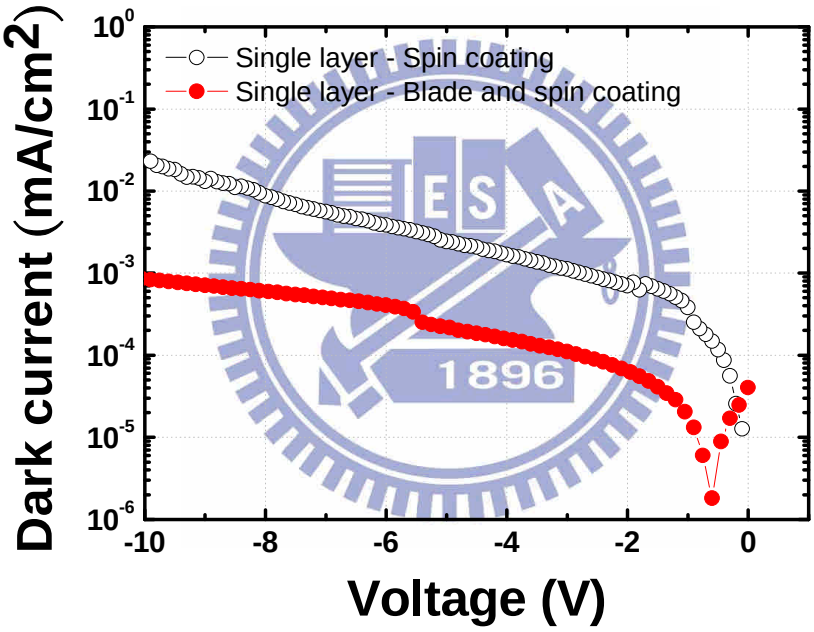

Fig. 8-1-c The J-V characteristics of single layer photo-detector by spin coating and blade and spin coating

8.2 Multilayer photo-detectors with PCBM as hole blocking layer

8.2.1 Bilayer structures

Fig. 8-2-a, the bilayer devices with general annealing process to evaporating the remains solvent by blade coating (dark line), it seems the serious dissolution according to reduce performance with high dark current about 6.1×10^{-4} mA/cm^2. The bilayer device with the spin-rinsed process (red line) has low dark current of 3.8×10^{-4} mA/cm^2 at -3V. The device is 15 times lower than the device with dissolution problem. Furthermore we use the annealing temperature 200℃ in spin-rinsed process to fabricate the device with lowest dark current about 3.0×10^{-5} mA/cm^2 at -3V than the spin-rinsed device. It is very important to reduce dissolution problem between polymer layers.

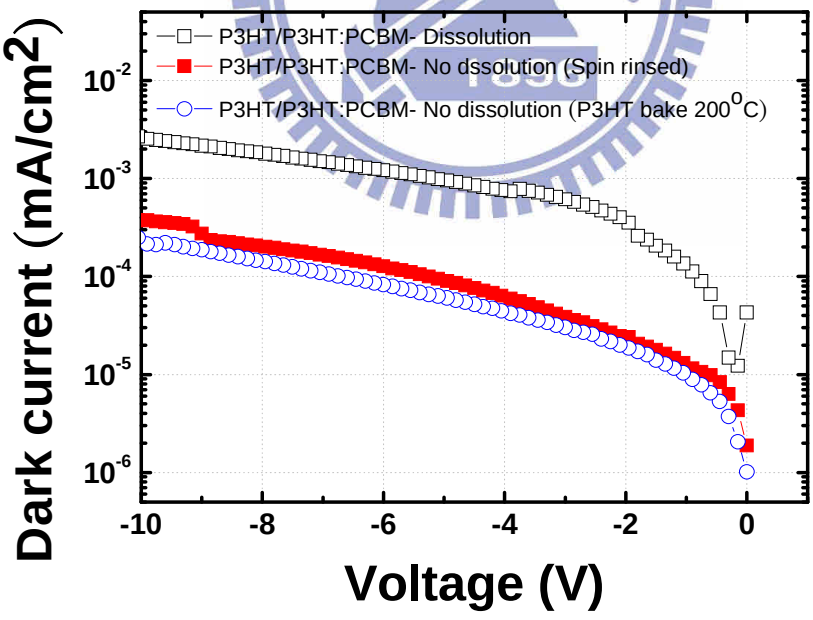

Fig. 8-2-a The J-V characteristics of bilayer structure P3HT/P3HT:PCBM

In addition, we design the different bilayer structures by blade and spin coating except the net PCBM are deposited by blade coating only, which are P3HT/PCBM, P3HT/P3HT:PCBM, and P3HT:PCBM/PCBM. The device performance is shown in Fig. 8-2-b, the P3HT/P3HT:PCBM device has the lowest dark current among the bilayer devices. It could achieve the bilayer structure of P3HT/P3HT:PCBM with low dark current since P3HT is easy to deposition by solution process, unlike PCBM. However the other bilayer devices do not have the low dark current as P3HT/P3HT:PCBM structure than single layer. The J-V characteristic of P3HT/PCBM device is almost equal with single layer device that can be attributed to the less separation interface between P3HT and PCBM elements. Another device with addition the PCBM layer as the HBL, that is complete no tendency of reduce the hole carrier injection from cathode. It is probably a consequence of the net small molecule to grow a stable thin film leading to destroy the preceding polymer layer to decrease the device performance.

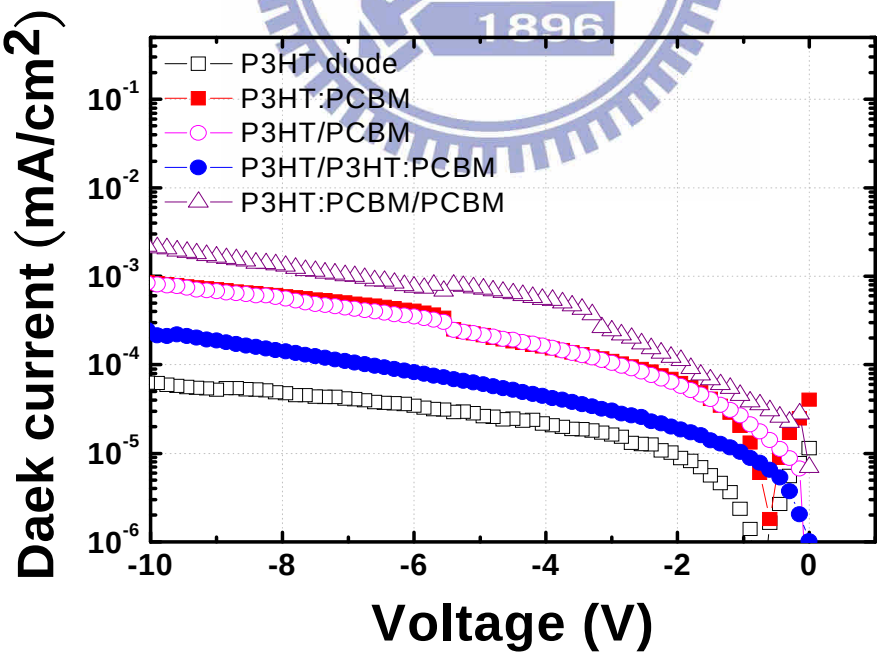

Fig. 8-2-b The J-V characteristics of three type's bilayer devices

8.2.2 Trilayer structure

Here we add an EBL ahead active layer and a HBL behead active layer. As Fig. 8-2-c shows the trilayer device with dark current about 2.6×10^{-5} mA/cm^2 at -3V. The result is almost similar to bilayer case of P3HT/P3HT:PCBM. The major difference may produce from the PCBM deposition problem. Until here in this study, we could not successful make a stable trilayer device to verify the hole blocking ability.

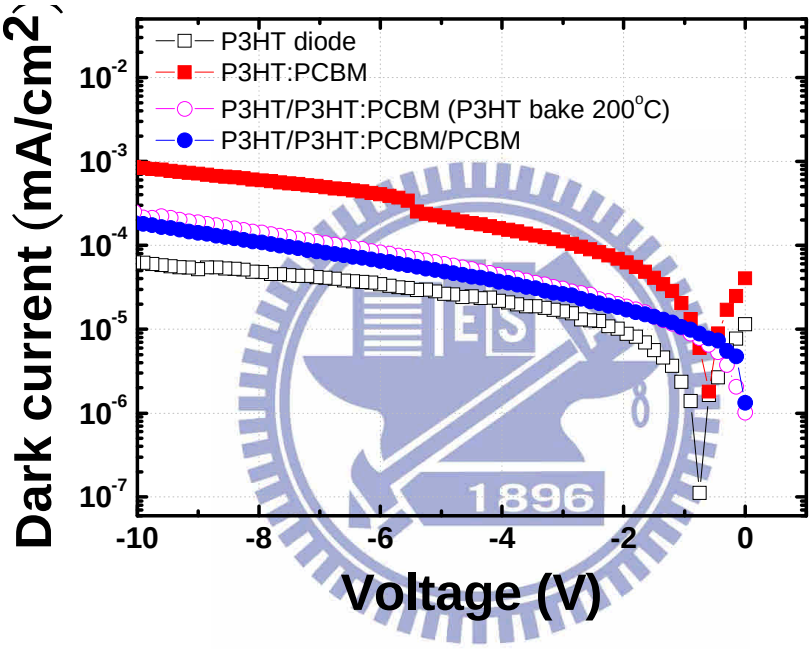

Fig. 8-2-c The J-V characteristics of the bilayer and trilayer devices with PCBM as HBL

Here we turn to discussion the on/off ratio between photocurrent (on current) and dark current (off current) of devices. The photocurrent is used to observe the conversion ability from incident photons to electrons under illuminant. And we choose the two types for incident wavelength are 550nm and 650nm which is included around P3HT absorption region. In order to effective separate the sensitivity of devices, we control the light intensity with a low lamp power about 5V, corresponding the power density are 1.8×10^{-6} W/cm^2 at 550 nm and 3.4×10^{-6} W/cm^2 at 650 nm respectively.

As shown in Fig. 8-2-d, the bilayer structure has excellent on/off ration since the clearly lower dark current than others. However the on/off ration of trilayer device is not great due to the device has the higher dark current with about 5.5×10^{-4} mA/cm^2 at -3V that is larger over twentyfold than bilayer case. From Fig. 8-2-d the bilayer and trilayer structures have the greater ratio than single layer may due to the net P3HT would be a good mobility to carrier transport. And the tendencies are similar of incident wavelength in 550 nm and 650 nm.

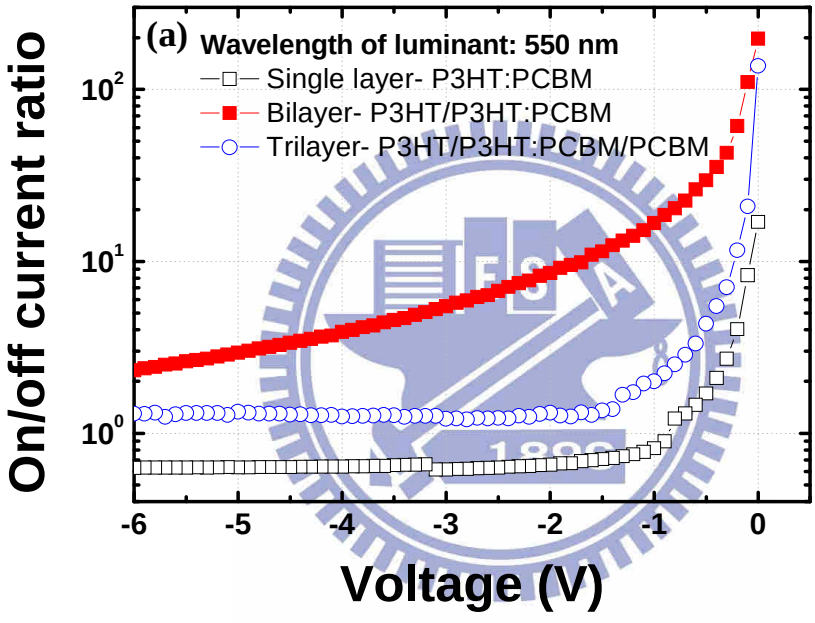

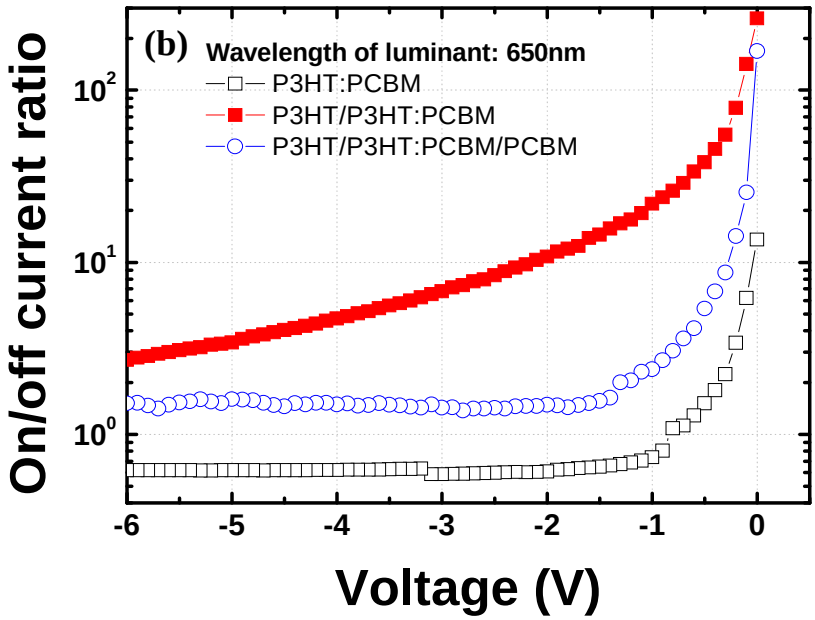

Fig. 8-2-d The on/off ratio of multilayer devices with incident wavelength (a) 550nm (b) 650nm

The incident photon-to-electron conversion efficiency (IPCE) implicates the conversion rate from photon energy of the photo-detector absorption to photocurrent. The general absorption wavelength is about 400 nm to 650 nm of 340 nm thickness for photo-detector. According the Fig. 8-2-e, the devices of bilayer and multilayer structures have the similar conversion efficiency as single layer with about 60 % at 0V in 540 nm wavelength. The important result shows the bilayer structure has the advantages of reducing dark current and no sacrifice the proper conversion rate. Furthermore the IPCE increases from 60% to 75% approximately by applying a reverse bias with -5V and -10V.

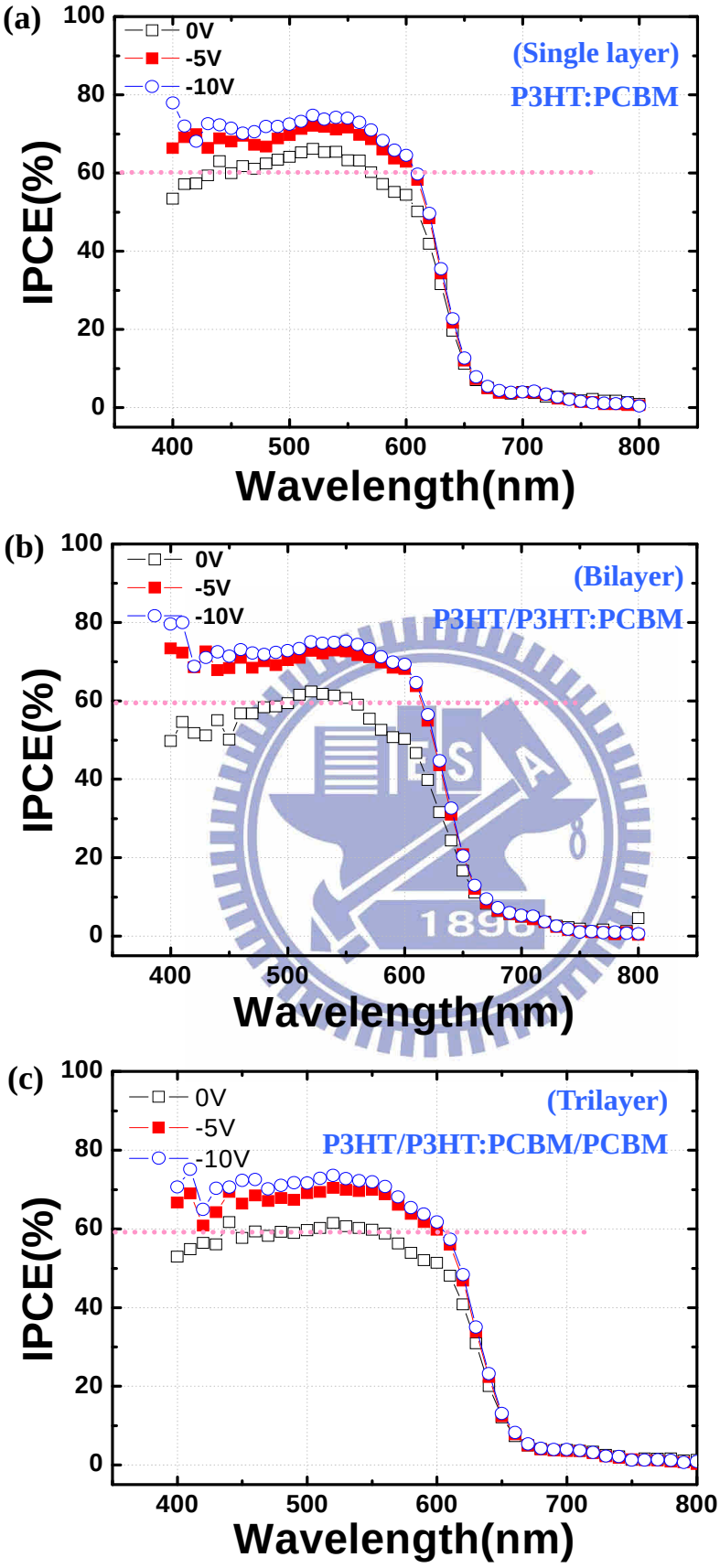

Fig. 8-2-e Schematic IPCE for (a) single layer, (b)bilayer, and (c) trilayer structures

In order to understand the sensitivity for photo-detector, we measure the frequency response with a light source of maximum frequency 4M Hz for inorganic LED shown in Fig. 8-2-f, Fig. 8-2-g, and Fig. 8-2-h. The frequency in 100k Hz is compared with single layer, bilayer, and trilayer devices. The single layer device is slightly better performances than multilayer devices with the degree of square wave. However all of the devices in the 100k Hz have the similar tendency that because the total thickness of the active layer is about the same with the nearly carrier mobility for devices. The results may illustrate that adding the EBL and HBL do not obvious influence the response. Furthermore the response waveform changes from square wave for low frequency to the sine wave for high frequency as shown the bilayer and multilayer devices with frequency variation from 100k Hz to 1M Hz in Fig. 8-2-g and Fig. 8-2-h.

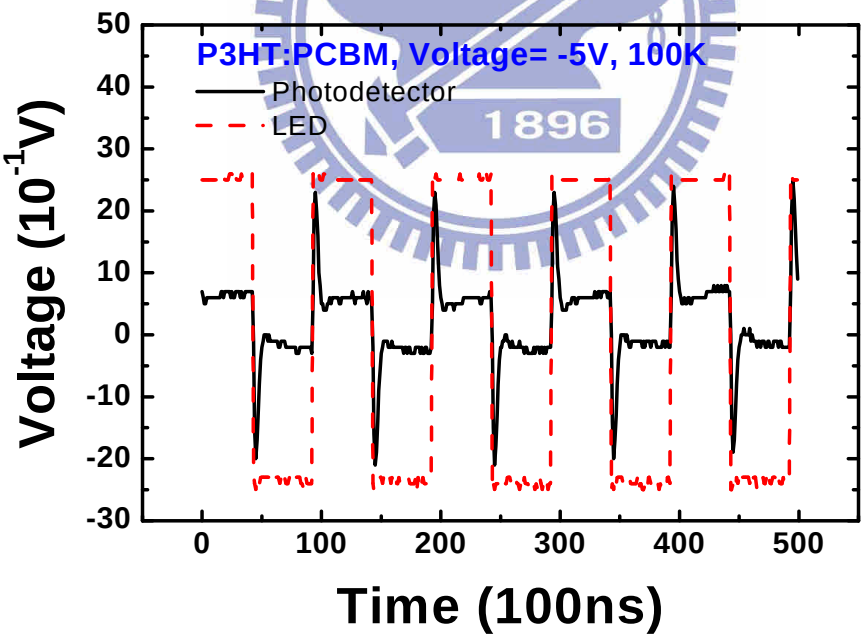

Fig. 8-2-f Frequency response of the single layer device with 100k Hz

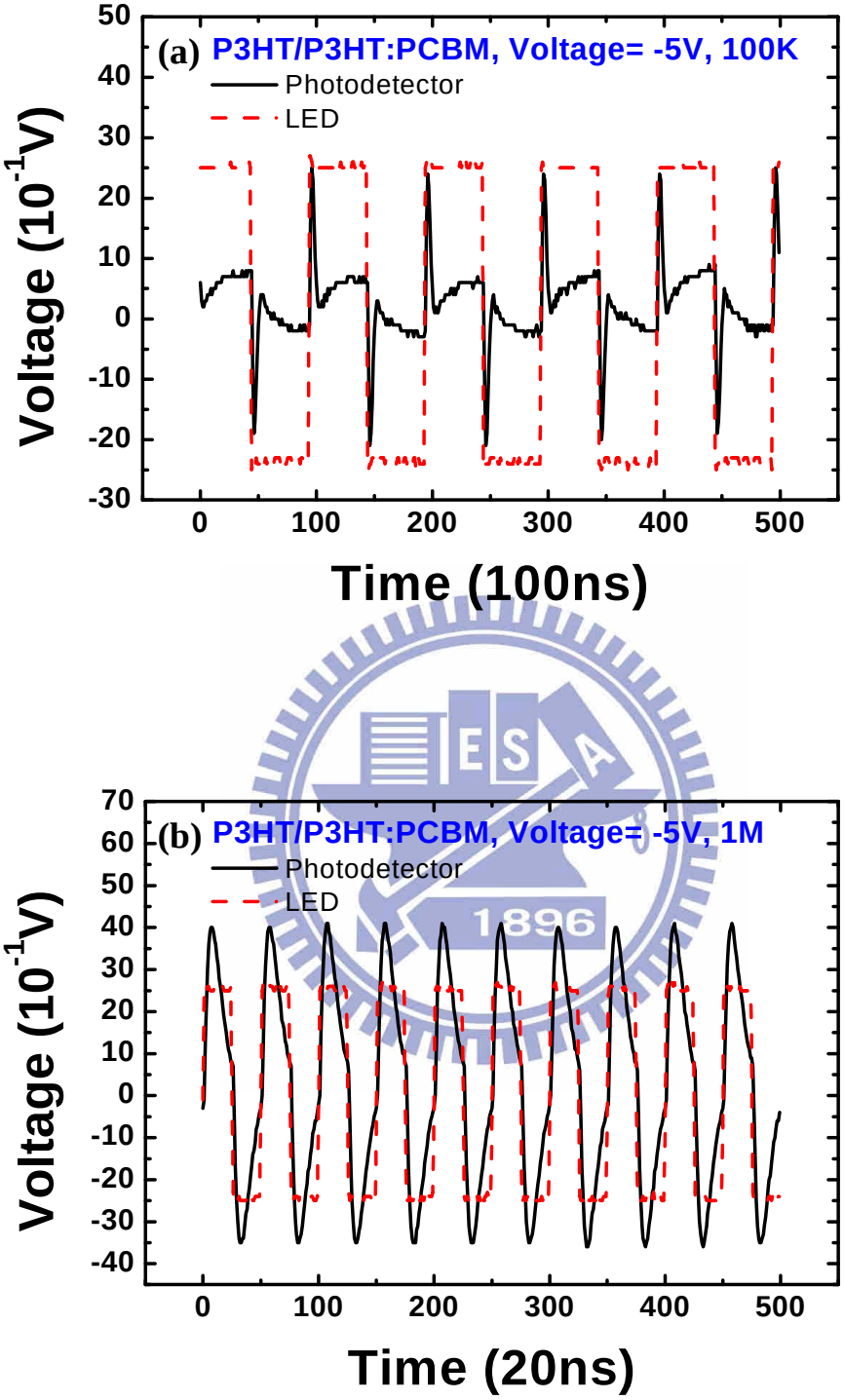

Fig. 8-2-g Frequency response of the bilayer device with (a) 100k Hz and (b) 1M Hz

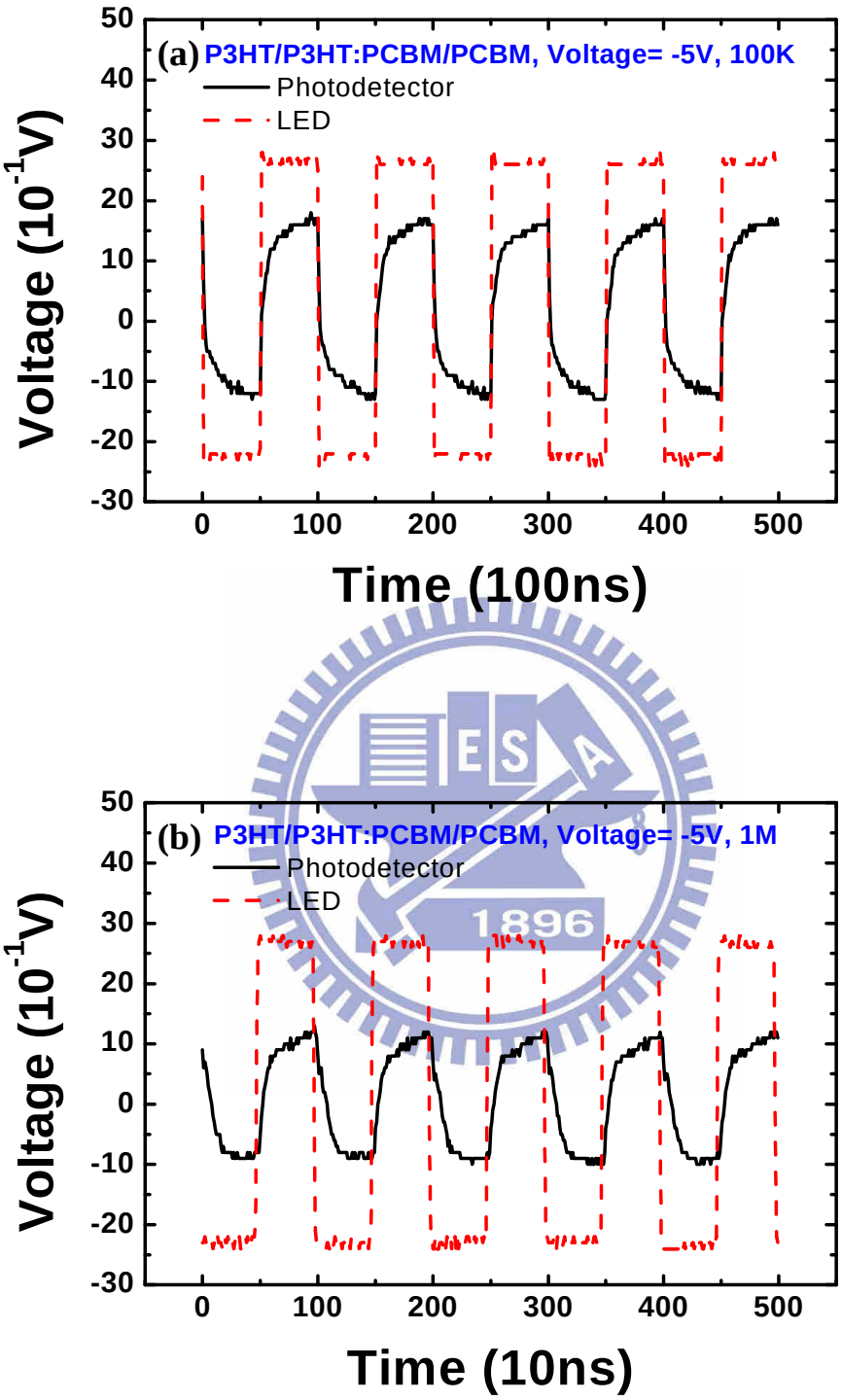

Fig. 8-2-h Frequency response of the PCBM trilayer device with (a) 100k Hz and (b) 1M Hz

8.2.3 Problems of PCBM layer

The multilayer structures are used the PCBM as the hole blocking layer to reduce dark current as shown in Fig. 8-2-c. However there is a remarkable problem of the small molecule PCBM is not easy to deposition thin film such as the Fig. 8-2-i (a). When depositing PCBM layer upon polymer layer would produce the serious dissolution between polymer layers as Fig. 8-2-i (b). The problem is produced the clearly influence on unable fabrication the stable multilayer device by PCBM.

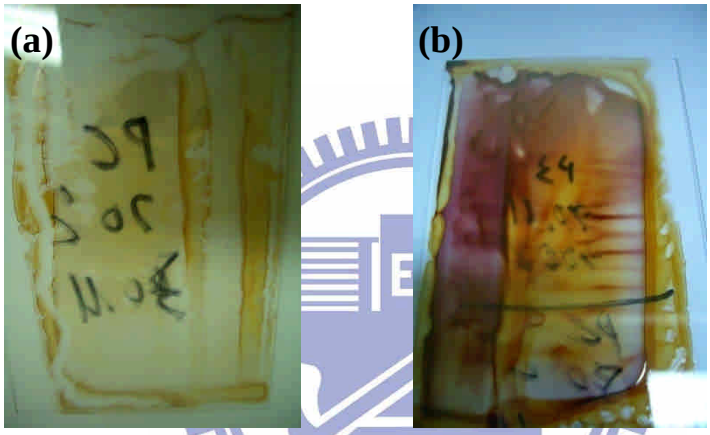

Fig. 8-2-i (a) Deposition the net PCBM film on the glass substrate (b) The serious dissolution problem between PCBM layer and polymer layer

8.3 Multilayer structures with BPhen as hole blocking layer

8.3.1 Bilayer structure

The bilayer structure is used BPhen material as the HBL as shown Fig. 8-3-a (blue line). The BPhen bilayer could reduce dark current to 4.3×10^{-5} mA/cm^2 that is approach the P3HT/P3HT:PCBM bilayer structure with 3.0×10^{-5} mA/cm^2 at -3V. The bilayer device of addition the EBL or HBL is the similar current values that seems the electron injection and the hole injection are the opposite important of dark current source.

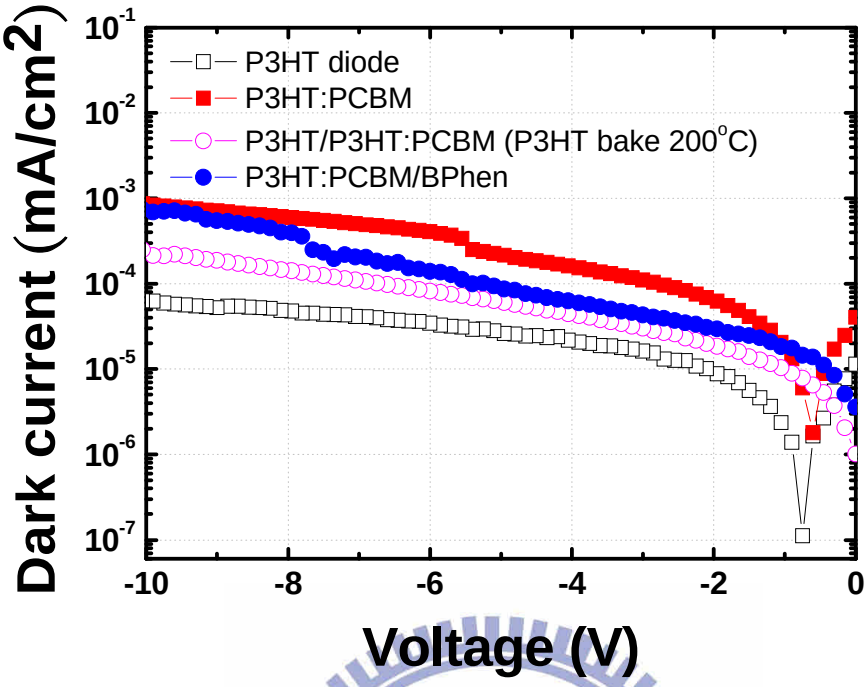

Fig. 8-3-a Schematic J-V characteristics of the bilayer device with using BPhen as HBL

8.3.2 Trilayer structure

For Fig. 8-3-b shows the bilayer and trilayer structure with BPhen as the HBL. The results to show the trilayer structure seems no clearly improvement of dark current. It is only reducing from 1.1×10^{-4} mA/cm^2 of single layer, but not low enough than bilayer devices. There is a major problem of deposition BPhen layer as the section 8-3-3.

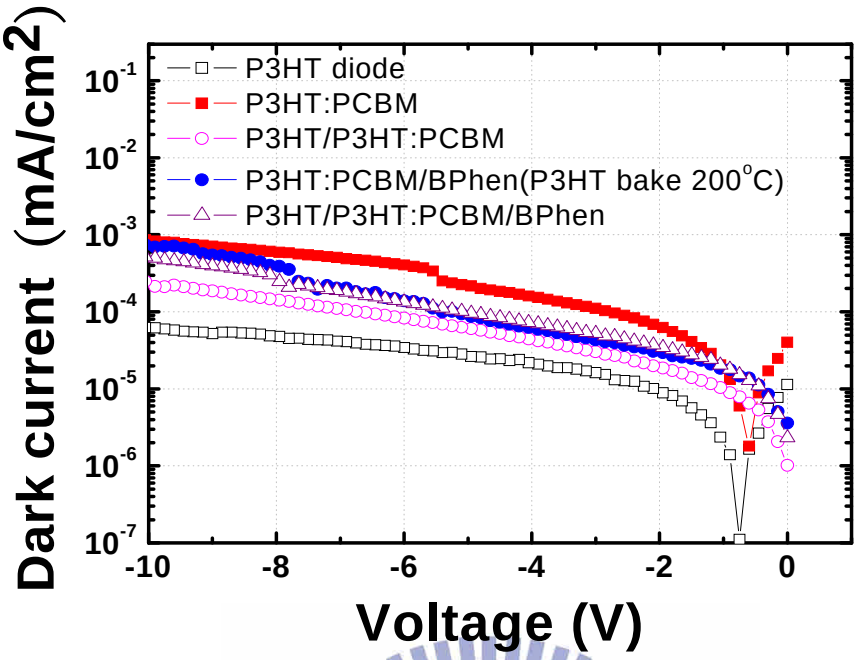

Fig. 8-3-b Schematic J-V characteristics of the trilayer device with using BPhen as HBL

The IPCE for BPhen trialyer device is shown in Fig. 8-3-c. As can be seen, the IPCE performance is a clear different with PCBM trilayer device as Fig. 8-2-e (c) at 0V. The trilayer BPhen device has the IPCE about 35% and the PCBM device is about 60% at 0V. When applying a small reverse bias, the IPCE of BPhen device would increase to 70% approximately that is similar with the performance for PCBM trilayer device. The absorption region is almost equivalent of each trilayer devices.

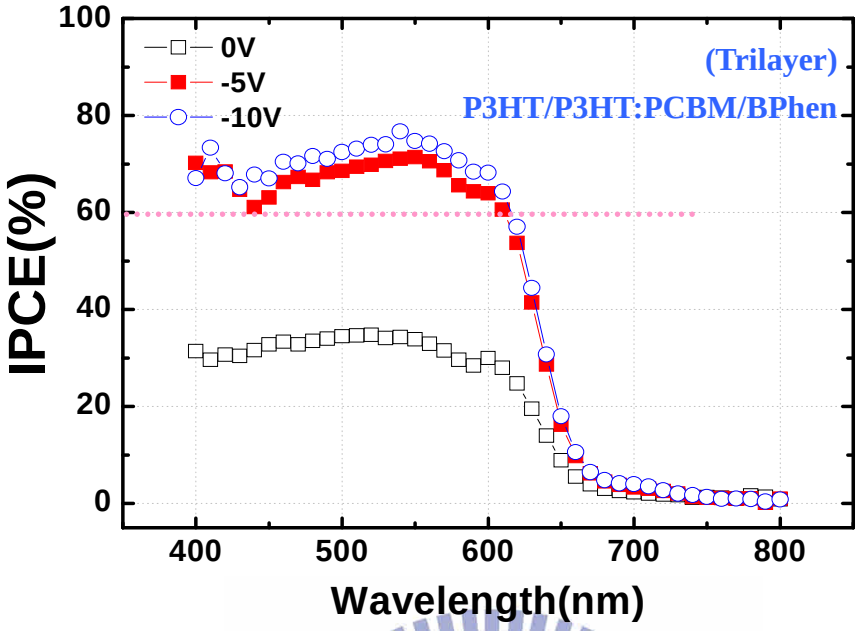

Fig. 8-3-c The IPCE of the trilayer device with using BPhen as HBL

For Fig. 8-3-d, we compare with 100k Hz and 1M Hz frequency response. The device is a good behavior with the nearly squire wave even the high frequency. Trilayer device has the similar response tendency with the PCBM trilayer device because of they have the almost same thickness of active layer.

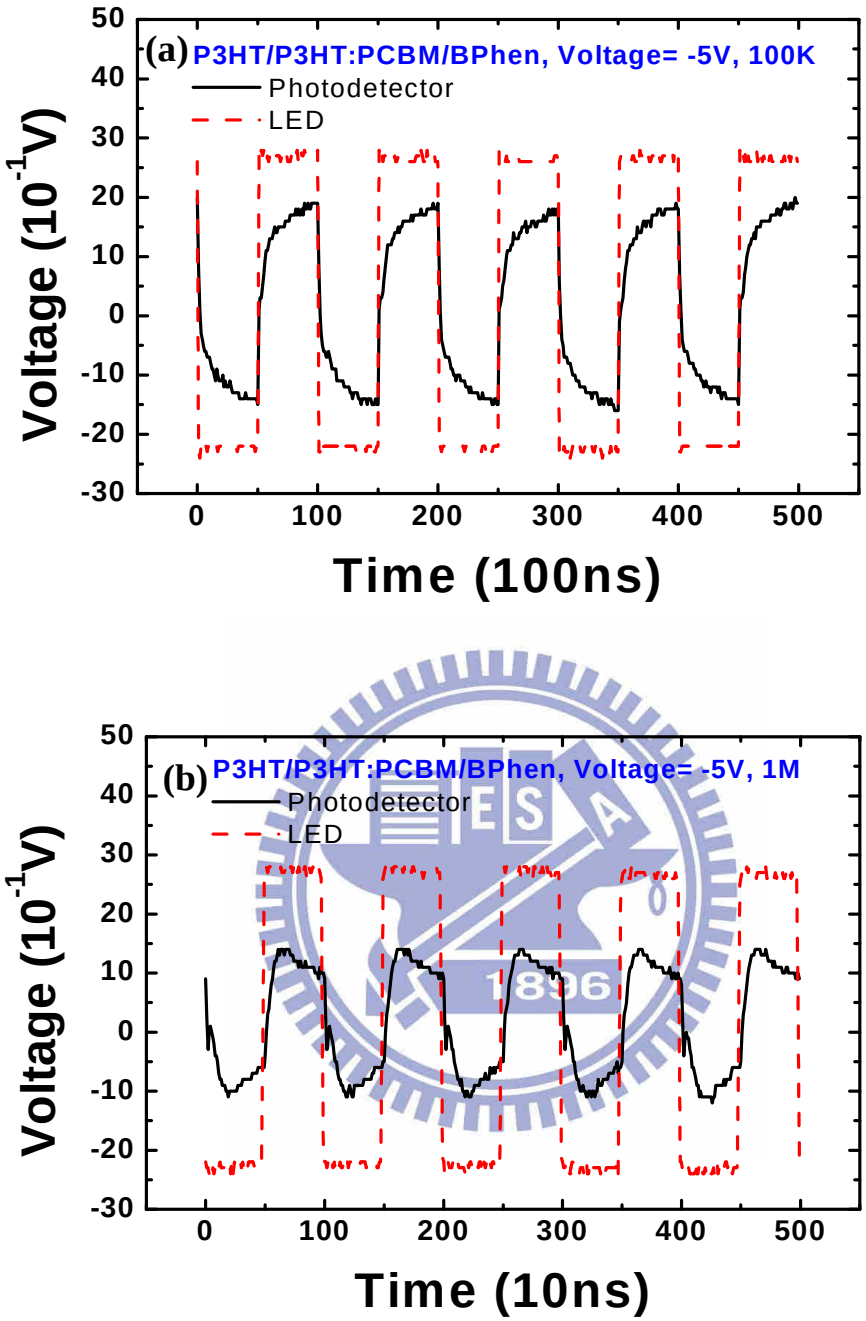

Fig. 8-3-d Frequency response of BPhen trilayer device with (a) 100k Hz and (b) 1M Hz

8.3.3 The problem of BPhen layer

The small molecular BPhen is dissolve in the hydrophile methanol solvent. The polar property of methanol has a main advantage of no dissolution between the polymer layers unlike net PCBM film. However there also existed the problem with deposition for small

molecules. The major reason is the small molecules do not have the function chains to grow a completely thin film by solution. Even constrained deposition by blade coating, which is a damaged layer such as a reticulation. So the BPhen could not develop the stable multilayer devices yet.

8.4 Next improvement

In general, the wavelength of illuminant and the absorption for polymer proximity sensor are almost in visible light that due to the properties of polymer material. Nevertheless the visible light is easy to be reduced the transmission message by scattering that attributes to the short luminance wavelength with the strong particle properties. Therefore the one of the important opinion about improvement the problem of the polymer proximity sensor is transformed the operation wavelength into near-infrared wavelength with clearly wave properties. This work will be proceeded to research in the next steps.

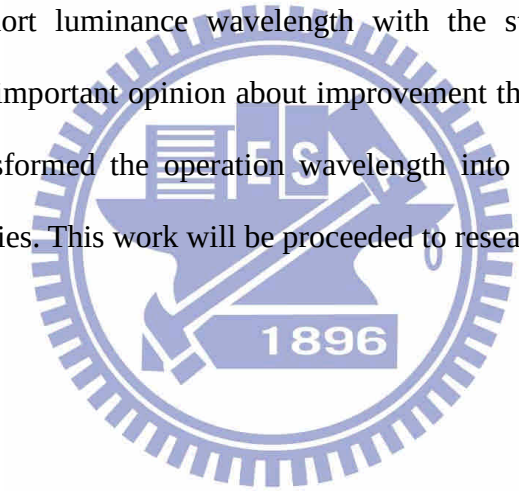

Chapter 9 Conclusion

In conclusion we use the blade coating to fabricate polymer photo-detectors with the low dark current of 10^{-5} mA/cm^2 as the summary table. The device structures are designed to multilayer, which are added electron blocking layer and hole blocking layer. Compare with single layer devices by spin coating there is the high sensitivity of multilayer photo-detectors.

Table 9-1 The summary of dark current for polymer photo-detector

Experiment	Layers	Structures	Voltage (V)	Dark current (mA/cm^2)
Spin coating	Single	P3HT:PCBM	-3	~10^{-3}
Blade coating	Single	P3HT:PCBM	-3	~10^{-4}
Blade coating	Bilayer	P3HT/P3HT:PCBM	-3	~10^{-5}
Blade coating	Multilayer	P3HT/P3HT:PCBM/PCBM	-3	~10^{-5}

References

[1] 張正華等編著，馬振基校訂，”Organic solor cell and plastics solar cells”，五南出版社 (2007).

[2] D. M. Chapin, C. S. Fuller, and G.L. Pearson, J. Appl. Phys. 25, 676 (1954).

[3] J. Zhao, A. Wang, and M. A. Green, Prog. Photovolt. : Res. Appl. 7, 471 (1999)

[4] D. E. Carlson and C. R. Wronski, “Amorphous silicon solar cell,” Appl. Phys. Lett. 28, 671 (1976)

[5] K. Sriprapa and P. Sichanugrist, Photovoltaic Energy Conversion, 2003. Proceedings of 3rd World Conference on Volume 3, Page(s):2799 - 2800 (2003)

[6] M. A. Contreras, B. Egaas, K. Ramanathan, J. Hiltner, A. Swartzlander, F. Hason, and R. Noufi, Res. Appl. 7, 311 (1999).

[7] R. McConnell, S. Kurtz, and M. Symko-Davies, Refocus. July/August (2005).

[8] K. M. Coakley and M. D. McGehee, Chem. Mater. 16, 4533 (2004).

[9] C. W. Tang, Appl. Phys. Lett. 48, 183 (1986).

[10] G. Yu, K. Pakbaz, and A. J. Heeger, Appl. Phys. Lett. 64, 3422 (1994).

[11] J. Nelson, Curr. Opin. Solid State Mater. Sci. 6, 87 (2002).

[12] G. Yu, A. J. Heeger, J. Appl. Phys. 78, 4510 (1995).

[13] J.J.M.Halls, C.A. Walsh, N.C. Greenham, E.A. Marseglia, R.H. Friend, S.C.Moratti, A.B. Holmes, Nature 376, 498(1995).

[14] Kyungkon Kim, Appl. Phys. Lett. 90, 163511 (2007).

[15] Holger Spanggaared, Frederik C. Krebs, Solar Energy Materials&Solar Cells 83, 125 (2004)

[16] G. Li, V. Shrotriya, J. Huang, Y. Yao, T. Moriarty, K. Emery, and Y. Yang, Nat. Mater. 4, 864 (2005).

[17] W. L. Ma, C. Y. Yang, X. Gong, K. Lee, and A. J. Heeger, Adv. Funct. Mater. 15, 1617

(2005).

[18] P. Schilinsky, C. Waldauf, and C. J. Brabec, Adv. Funct. Mater. 16, 1669 (2006)

[19] website of “Research Institute of Innovative Technology for the Earth, RITE” (http: //www.rite.or.jp/).

[20] B. O’Regan and M. A. Grätzel, Nature 353, 737 (1991)

[21] 陳婉如，”有機太陽電池技術開發與實用化進展” 光聯雙月刊 56 期，24-27 頁 (2005).

[22] W. L. Ma, C. Y. Yang, X. Gong, K. Lee, and A. J. Heeger, Adv. Funct. Mater. 15, 1617 (2005).

[23] C. N. Hoth, P. Schilinsky, S. A. Choulis, and C. J. Brabec, Nano Lett. 8, 2806 (2008).

[24] S. E. Shaheen, R. Radspinner, N. Peyghambarian, and G. E. Jabbour, Appl. Phys. Lett. 79, 2996 (2001).

[25] K.X. Steirer, M.O. Reese, B.L. Rupert, N. Kopidakis, D.C. Olson, R.T. Collins, D.S. Ginley, Sol. Energy Mater. Sol. Cells 93 (2009) 447.

[26] P. Schilinsky, C. Waldauf, and C. J. Brabec, Adv. Funct. Mater. 16, 1669 (2006).

[27] S.-S. Kim, S.-I. Na, J. Jo, G. Tae, D.-Y. Kim, Adv. Mater. 19, 4410 (2007).

[28] P. Schilinsky, C. Waldauf, and C. J. Brabec, Adv. Funct. Mater. 16, 1669 (2006).

[29] S. R. Tseng, K. C. Lee, H. F. Meng, S. F. Horng, Appl. Phys. Lett. 93, 153308 (2008).

[30] W. U. Huynh, J. J. Dittmer, G. Whiting, W. Libby, and A. P. Alivis atos, Adv. Funct. Mater. 13, 73 (2003).

[31] 莊嘉琛, 太陽能工程–太陽電池篇, 金華科技圖書股份有限公司, (1997).

[32] H. Hoppe, N. S. Sariciftci, J. Mater. RES., Vol. 19, No. 7 (2004)

[33] H. Sirringhaus, P. J. Brown, R. H. Friend, M. M. Nielsen, K. Bechgaard, B. M. W. Langeveld-Voss, A. J. H. Spiering, R. A. J. Janssen, E. W. Meijer, P. Herwig, and D. M. de Leeuw, Nature, 401, 685 (1999).

[34] Y. Zhao, Z. Xie, Y. Qu, Y. Geng, and L. Wang, Appl. Phys. Lett. 90, 043504 (2007).

[35] X. Yang, J. Loos, S. C. Veenstra, W. J. Verhees, M. M. Wienk, J. M. Kroon, M. A. J. Michels, and R. A. J. Janssen, Nano Lett. 5, 579 (2005).

[36] M. Pope， H.P. Kallmann， P. Magnante， J. Chem. Phys. 38, 2042 (1963).

[37] C.W. Tang， S.A. VanSlyke， Appl. Phys. Lett. 51 , 913 (1987).

[38] E. S. Zaus, S. Tedde, T. Rauch, J. Fürst, G. H. Döhler, IEEE T Electron dev. 55, 2 (2008).

[39] G. Li, V. Shrotriya, J. huang, Y. Yao, T. Moriarty, K. Emery, Y. Yang, Nat. Material 4, 864 (2005).

[40] S. R. Tseng, H. F. Meng, C. H. Yeh, H. C. Lai, S. F Horng, H. H. Liao, C. S. Hsu, L. C. Lin, Synth. Met. 158, 130-134 (2008).

[41] L. Chen, P. Degenaar, D. D. C. Bradley, Adv. Mater 20, 1679 (2008).

[42] S. R. Tseng, H. F. Meng, K.C. Lee, S. F. Horng, Appl. Phys. Lett. 93, 153308 (2008).

[43] J. S. Kim, R. H. Friend, I. Grizzi and J. H. Burroughes Appl. Phys. Lett. 87, 023506 (2005).